

Established DFT methods calculation of conjugation disturbed in the presence of torsional hyperconjugation

John N. Sharley, University of Adelaide

john.sharley@pobox.com

arXiv:1512.04171

Abstract

Accurate treatment of amide resonance is important in electronic structure calculation of protein, for Resonance-Assisted Hydrogen Bonding [1-3], RAHB, in the hydrogen bonded chains of backbone amides of protein secondary structure types such as beta sheet [4] and alpha helix [5] is determined by amide resonance. Variation in amide resonance is the means by which the hydrogen bonding in these chains is cooperative.

Amide carbonyl orbitals are revealed by Natural Bond Orbital [6-8], NBO, analysis to substantially maintain sigma/pi separation in the presence of torsional hyperconjugative [6] interactions with wavefunction methods but not with established Density Functional Theory [9, 10], DFT, methods. This DFT error is most pronounced with small basis sets such as are used with DFT for proteins to reduce the basis function count. This error disturbs calculation of a range of amide donor-acceptor and steric interactions.

This finding has important implications for the selection of electronic structure methods and basis sets for protein calculations. For example, great caution is needed in interpreting the results of applying established DFT methods to proteins containing beta sheet. We recommend that every protein DFT calculation be accompanied by NBO assessment of maintenance of amide carbonyl sigma/pi separation and absence of carbonyl bond bending. Further, we propose that these metrics be standard benchmarks of electronic structure methods and basis sets.

Notation

“->” denotes NBO resonance-type charge transfer and “|” denotes NBO steric exchange repulsion. “(“ and “)” enclose specification of an orbital type and follow an atom name for single-center NBOs and a pair of atom names separated by “-” for two-center NBOs.

Examples: N(lp) for the amide nitrogen lone pair NBO, O(lp-p) for the oxygen p-type lone pair NBO, O(lp-s) for the s-rich lone pair NBO, C-O(p)* for the pi carbonyl antibonding orbital NBO and N(lp)->C-O(p)* for the primary amide resonance type charge transfer.

Overview

NBO analysis provides an optimal account of correlated electron density which is useful for determining differences in electron density. Differences in NBO-derived quantities are not arbitrary with respect to electron density. NBOs are not unitarily equivalent to molecular orbitals [11].

NBO is not committed to maintenance of sigma/pi separation of orbitals of multiple bonds. The NBO account of sigma/pi separation varies according to electron density. NBO analysis may reveal loss of sigma/pi separation in the presence of angular strain or chemical bonding. In the case of double

bonds having hyperconjugative interactions, there exists a significant difference between the electron density calculated by established DFT methods versus MP2 [12] and in the extent of sigma/pi separation. This context is not particularly multireference. MP2 largely maintains sigma/pi separation and absence of bond bending, while DFT methods show large variation in the extent of sigma/pi separation and bond bending. This DFT error is sensitive to basis set and in vinylamine is reduced at the correlation consistent basis set [13] level Aug-cc-pV5Z but remains significant at Aug-cc-pV6Z.

Calculated amide electronic interactions disturbed by this error are not limited to loss of sigma/pi separation and carbonyl bond bending, and include variation of charge transfer from the nitrogen lone pair to carbonyl antibonding orbitals and steric interactions $C-O(s) | C-O(p)$, $O(lp-s) | C-O(s)$ and $O(lp-s) | C-O(p)$.

Vinylamine, ethanamide and polyvaline and polyalanine antiparallel beta sheet are used for these investigations. Ethanamide is used as a minimal example of the amide group having hyperconjugative interactions with the carbonyl group. Results of applying 43 non-double hybrid DFT [14, 15] methods in combination with 9 basis sets are reported. That these DFT issues also apply to protein beta sheet is shown with LC-wPBE [16], though these issues are not limited to that method.

Reduction of sigma/pi separation and increase in bond bending in the amide carbonyl group gives a reduction in calculated amide resonance. This necessarily means that RAHB of hydrogen-bonded chains of protein backbone amide groups is inaccurately calculated. RAHB is cooperative, and errors in calculated amide resonance may also be regarded as cooperative.

These findings have important implications for the selection of electronic structure methods for protein structure. Depending on method/basis set, any calculation of a range of internal amide electronic interactions may have a surprisingly large error. Results of calculation of cooperativity in backbone amide hydrogen bond, HB, chaining in beta sheet using DFT will be significantly in error even when medium size basis sets are used, and in practice small basis sets have been used due to the secondary structure atom and basis function count. Hyperconjugative interactions with the backbone amide carbonyl group occur in other hydrogen bonded secondary structure types, so this warning applies to proteins generally. Also, we have observed but do not otherwise report on variability in the amino-acid residue-specific extent of loss of sigma/pi separation and increase in bond bending. We recommend that every DFT calculation of protein be accompanied by NBO assessment of the extent of amide carbonyl sigma/pi separation and bond bending.

These findings lead to the proposal that these molecular situations be regarded as standard benchmarks of electronic structure methods and basis sets, and be used for refining parameter values where a method takes parameters.

A second kind of error arising from double bonds having hyperconjugative interactions is also reported here. This second error applies to the amide group, and results in pyramidalization at the amide nitrogen. It occurs depending on basis set when using wavefunction methods. The result of this error may be seen in coordinate geometry, though NBO may be used to quantitate the extent of the shift of nitrogen from sp^2 to sp^3 hybridization. This error is similar to the benzene non-planarity failures arising from negative out-of-plane bending frequencies reported in [17]. This error also reduces amide resonance since the nitrogen sp^3 hybridization is necessarily in competition with amide resonance. The above remarks about accuracy in calculations of RAHB also apply to this error. This second error is corrected by geometry optimization on the Counterpoise Correction [18] potential energy surface with fragment boundary defined at the C-N bond of ethanamide, but not at the C-C bond.

Introduction

The Natural Bond Orbital analysis procedure has properties that particularly recommend it for the analysis of electron density. Natural orbitals are natural in the sense of being the best possible account of correlated electron density [6], which suggests their use as the standard form for comparison of electron density. The localization of natural orbitals without loss of information as is done by NBO increases suitability for this purpose. NBO is usually directed to analysis with maximum transferability across molecular contexts, but here we use NBO to analyse the electron density resulting from different methods as applied to the same molecule, a somewhat different use of NBO's analysis of similarity.

In the present study we focus in particular on the Natural Hybrid Orbitals [6], NHOs, for these describe bond bending and sigma, pi and higher angular momentum character of bonds. There is no built-in bias or geometric preconception embedded in NHO description of bonds, and all aspects of hybridization are converged to an optimal description of electron density [6]. The NBO account of electron density can report reduction in sigma/pi separation and increase in bond bending, depending on the electron density. Differences in NBO-derived quantities are not arbitrary with respect to electron density. NBOs are not unitarily equivalent to molecular orbitals [11].

Comparing NBO with other means of assessing electron density differences: other chemical bonding analyses do not have a localized natural orbital basis. Density Difference Representation [19] is not oriented to chemical bonding and so the chemical significance of density change is not available.

We used NBO to quantitate the extent of sigma/pi separation and bond bending in double bonds having hyperconjugative interactions in vinylamine, ethanamide and antiparallel beta sheet. In vinylamine and ethanamide, torsion is constrained across the single bond central to hyperconjugation during geometry optimization. In beta sheet, no constraints during geometry optimization are necessary to maintain the torsion for non-planar hyperconjugation. The surveys reported here use constrained ethanamide as a model for protein backbone amide groups, and relevance of this model is supported by NBO analysis of fully optimized polyalanine and polyvaline protein secondary structures.

Backbone amide resonance is central to RAHB in protein backbone amide hydrogen bond chaining of certain protein secondary structure types including beta sheet. Accurate calculation of the RAHB cooperativity is important in calculating protein electronic structure and geometric structure.

Methods

Methods used in experiments are as implemented by Gaussian 09 D.01 [20], Orca 3.0.3 [21-23] and TeraChem 1.5K [24-27].

A pre-release version of NBO [28] was used for its XML [29] output option. The XML was queried with XQuery 3.0 [30] or XSLT 3.0 [31] as implemented by Saxon-PE 9.6.0.4 [32], and the results imported into Excel 2013 [33].

Jmol 14.2.2_2014.06.29 [34] was used for visualization of orbitals.

Results and discussion

Vinylamine

The results appearing in [6] of loss of sigma/pi symmetry in vinylamine at 10 degree C-C-N-H Torsion with B3LYP [35] /6-311++G** are in accord with our results (Figure 1 and Ap1:Figure 25). However, the ~20% loss of p character with B3LYP becomes less than 1% at MP2 (Ap1:Figure 23 and Ap1:Figure 25). Only with the smallest basis sets used, 6-31G** and Def2SVP, does the loss of p character with

MP2 approach 1%, and with other basis sets is \sim 0.5%. Of the basis sets used, 6-311++G** gives the least loss of p character with MP2.

The C-C NBO morphologies for B3LYP/6-311++G** and MP2/61-311++G** can be seen in Figure 6 to Figure 13. These graphics are for 10 degree torsion, which we use for commonality with [6], though greatest loss of sigma/pi symmetry is found at 15 to 30 degrees hyperconjugative torsion depending on basis set except for Aug-cc-pVTZ (Figure 1 and Ap1:Figure 23).

NHO deviation from line of centers, bond bending, also differs significantly between DFT methods and wavefunction methods. These deviations are charted as Figure 2, Ap1:Figure 24 and Ap1:Figure 26. For the C-O(pi) NHOs, 90 degrees is no deviation from expectation based on line of centers. For some basis sets with B3LYP the bond bending is as large as 45 degrees from the reference 90, contrasted with the 7 degree maximum bond bending with MP2.

Differences in the polarization of the C-O(sigma) and C-O(pi) NBOs is shown in Ap1:Figure 27 and Ap1:Figure 28. The variable performance of different DFT methods with Aug-cc-pVTZ can be seen. Broadly, Aug-cc-pVTZ is most associated with greatest difference between DFT methods, and between DFT methods and wavefunction methods. Aug-cc-pVDZ offers markedly less DFT divergence, which is frequently observed in this work. As always in this work, there is greatly less divergence between properties calculated with correlated wavefunction methods than with DFT methods.

The B3LYP and MP2 results are dichotomous, and nomination of which is in such large error is most desirable. It is not a given at the outset that the error is with B3LYP, for DFT methods are in principle capable of incorporating static correlation and uncorrected MP2 is not. In answering this question we refer to the results of other DFT methods including double hybrid methods [14], corrected MP2 methods [36, 37], DLPNO-CCSD(T) [23] and the multireference MRCI+Q [38], and note that B3LYP loss of symmetry begins to collapse at very large basis sets starting at Aug-cc-pV5Z (Figure 3 to Figure 5).

Ap1:Figure 25 to Ap1:Figure 28 show sigma/pi symmetry, bond bending and polarization at a range of DFT methods including hybrid methods, long-range corrected methods [39] and double hybrid methods, and some corrected MP2 methods, the invariably worst-performing method HF [34] and single point calculation at DLPNO-CCSD(T). The double hybrid [14] methods tested have only twice the error of MP2, but computational cost scales similarly.

The poor performance of HF and single hybrid methods and better performance of double hybrid and MP2 variants suggests an underlying mechanism of these errors, that being different treatment of multicenter exchange delocalization. DFT single hybrid and GGA exchange does not have multicenter delocalization, HF's multicenter exchange delocalization is uncorrected, MP2's correlation largely corrects HF's excessive multicentre delocalization [40] and double hybrid DFT's correction by correlation is not quite as good as MP2's.

We anticipate that with optimization at CCSD [41] or above, the loss of p character will be further reduced from the already small MP2 figure. Where DLPNO-CCSD(T) has been used in this work, it has necessarily been used for single point energy calculation, with geometry optimization at MP2/Aug-cc-pVQZ.

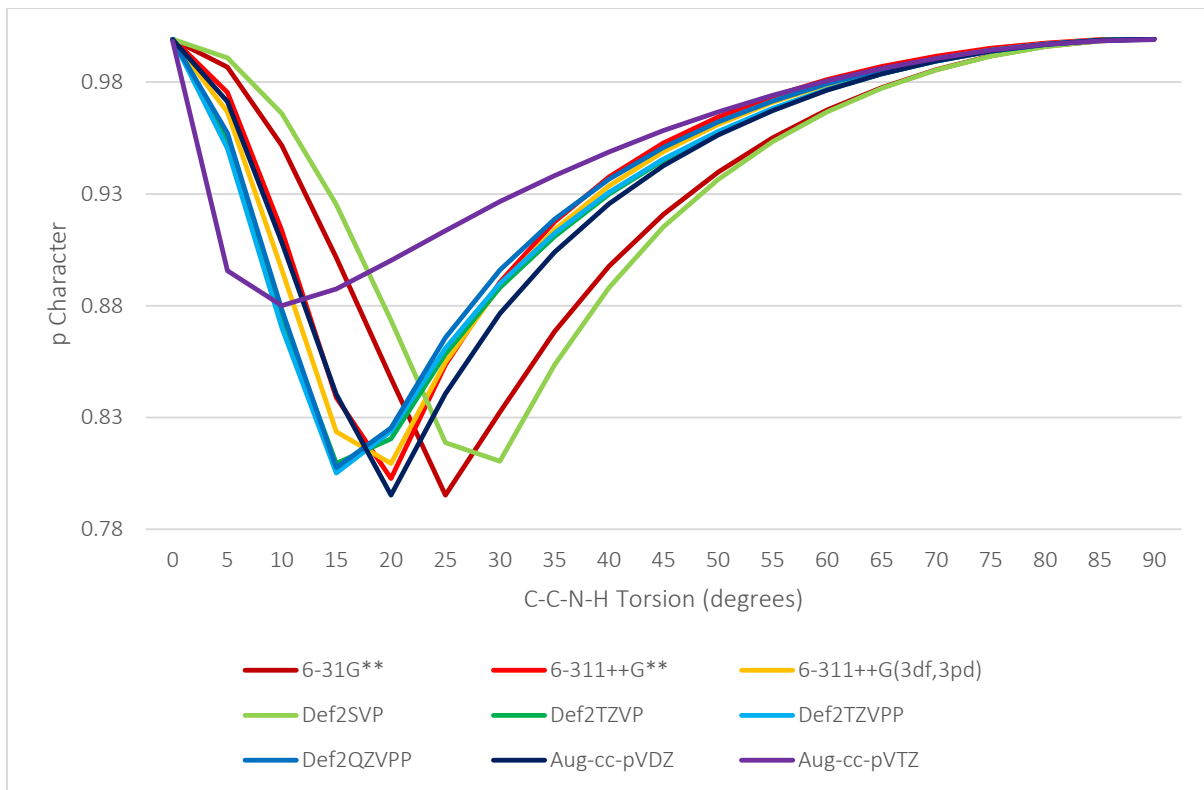


Figure 1. *C-C(pi)* Central Carbon NHO *p* Character in Vinylamine at Varying C-C-N-H Torsion and Basis Set at B3LYP

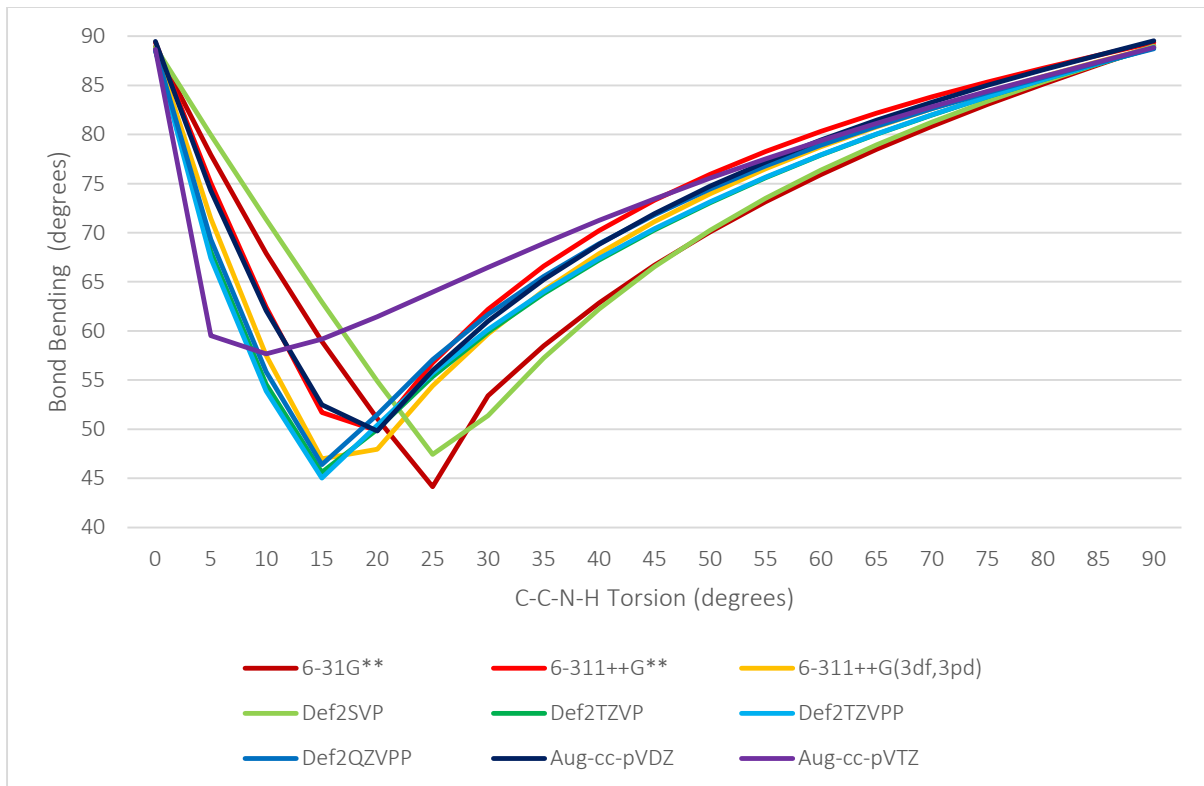


Figure 2. *C-C(pi)* Central Carbon NHO Bond Bending in Vinylamine at Varying C-C-N-H Torsion and Basis Set at B3LYP

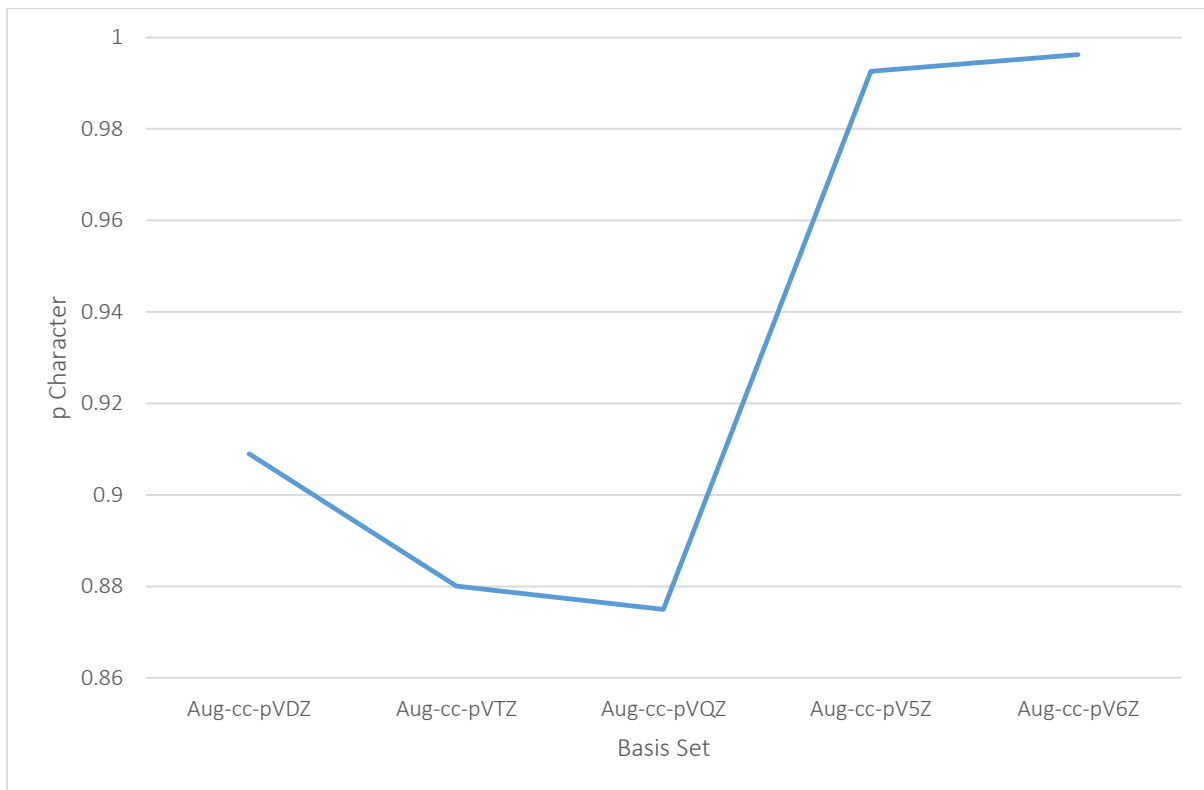


Figure 3. C-C(π) Central Carbon NHO p Character in Vinylamine at 10 Degree C-C-N-H Torsion with B3LYP and Varying Basis Set

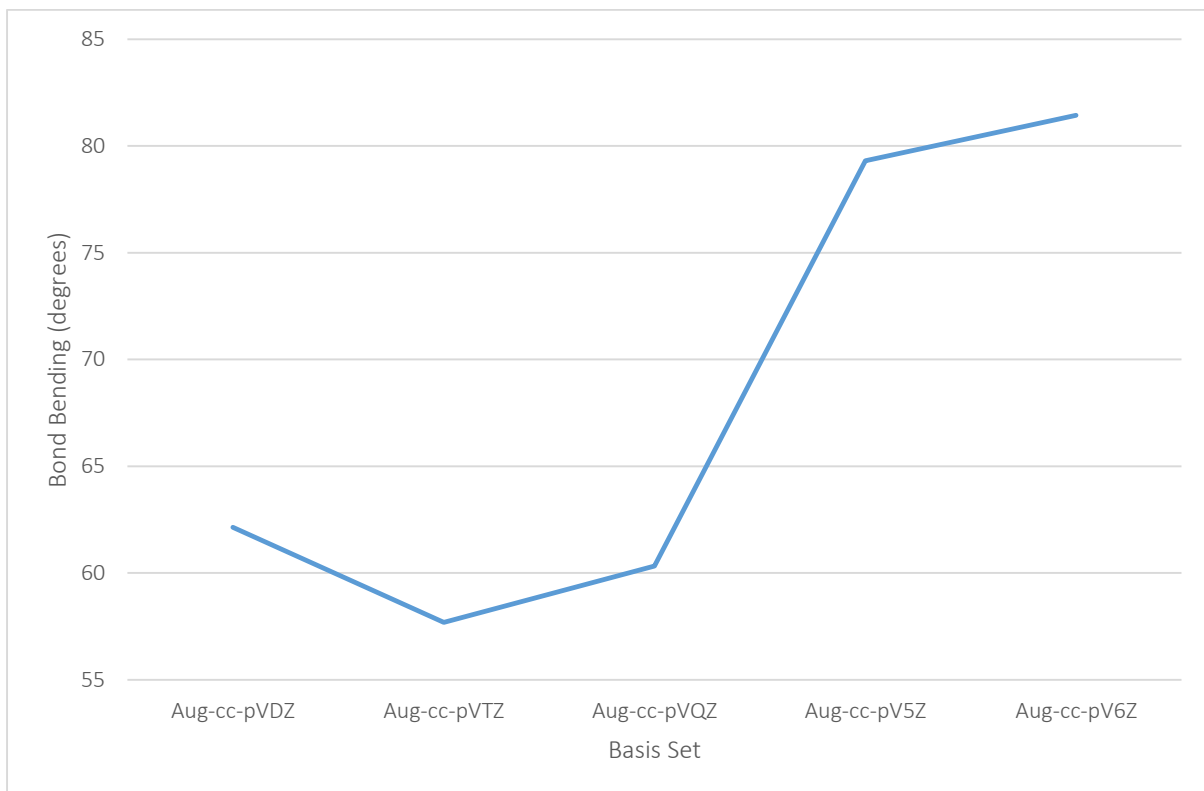


Figure 4. C-C(π) Central Carbon NHO Bond Bending in Vinylamine at 10 Degree C-C-N-H Torsion with B3LYP and Varying Basis Set

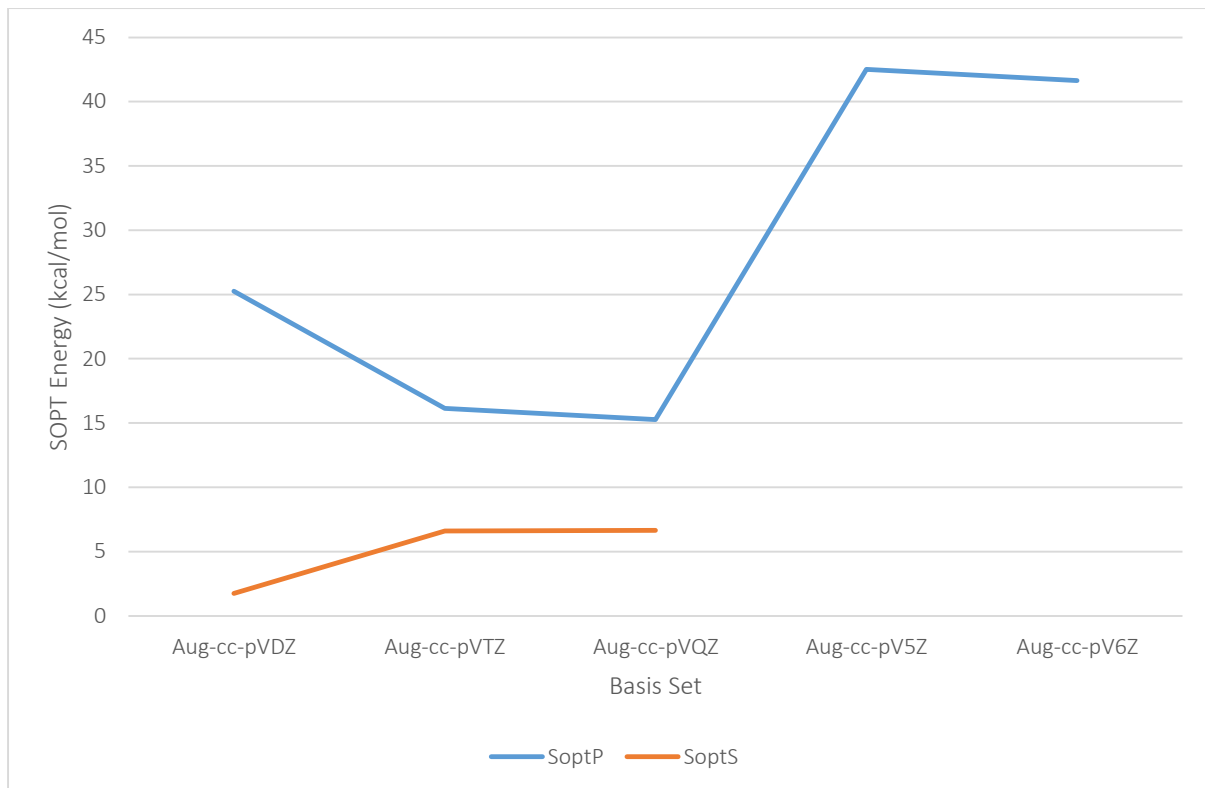


Figure 5. $N(p)\rightarrow C-C(\pi) \text{ then } \sigma^*$ SOPT Energy in Vinylamine at 10 Degree Torsion with B3LYP and Varying Basis Set

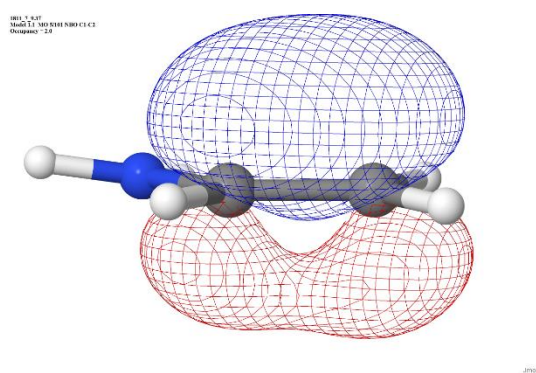


Figure 6. B3LYP/6-311++G** C-C(π) NBO in Vinylamine at 10 Degree C-C-N-H Torsion

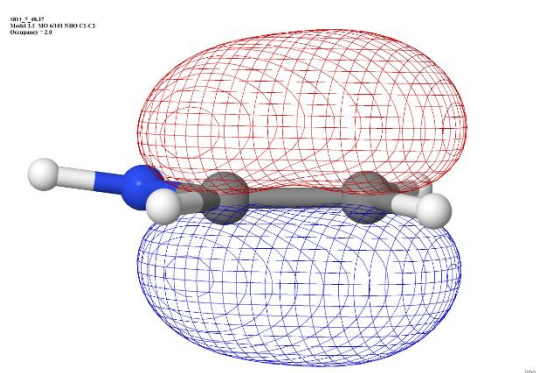
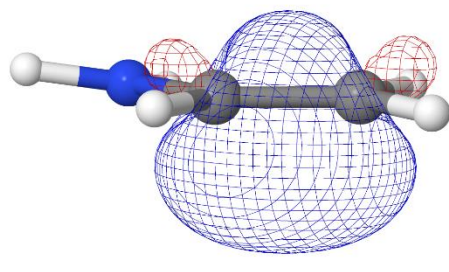


Figure 7. MP2/6-311++G** C-C(π) NBO in Vinylamine at 10 Degree C-C-N-H Torsion

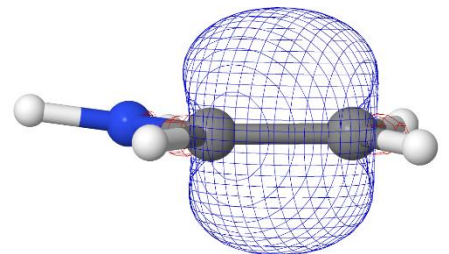
0011_3.sdf
Model 11 MO MO NBO NBO C1C2
Opacity: 24



.Jmol

Figure 8. B3LYP/6-311++G** C-C(sigma) NBO in Vinylamine at 10 Degree C-C-N-H Torsion

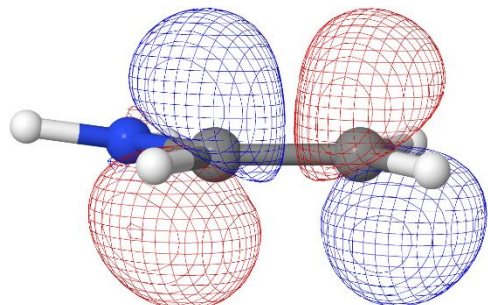
0011_3.sdf
Model 11 MO MO NBO NBO C1C2
Opacity: 24



.Jmol

Figure 9. MP2/6-311++G** C-C(sigma) NBO in Vinylamine at 10 Degree C-C-N-H Torsion

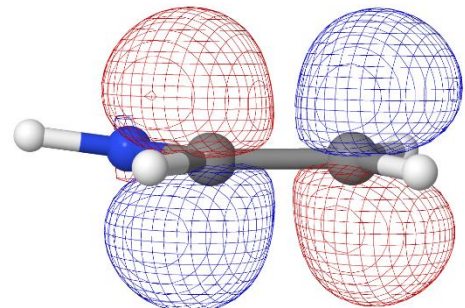
0011_3.sdf
Model 11 MO MO NBO NBO C1C2
Opacity: 62



.Jmol

Figure 10. B3LYP/6-311++G** C-C(pi)* NBO in Vinylamine at 10 Degree C-C-N-H Torsion

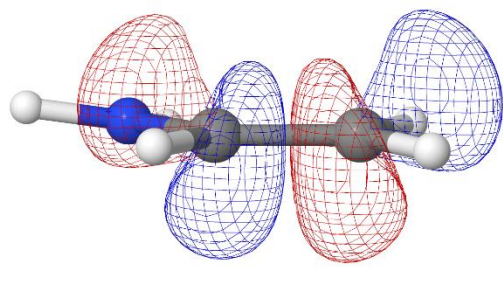
0011_3.sdf
Model 11 MO MO NBO NBO C1C2
Opacity: 62



.Jmol

Figure 11. MP2/6-311++G** C-C(pi)* NBO in Vinylamine at 10 Degree C-C-N-H Torsion

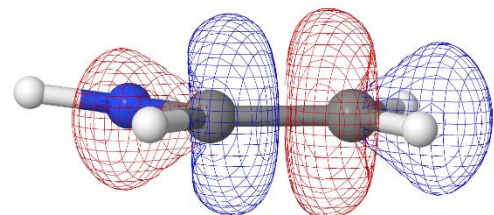
0011.3.487
Model 11 MO 10/01 NBO CH2C2
Occupancy = 0.8



Jmol

Figure 12. B3LYP/6-311++G** C-C(σ)* NBO in Vinylamine at 10 Degree Torsion

0011.3.487
Model 11 MO 10/01 NBO CH2C2
Occupancy = 0.8



Jmol

Figure 13. MP2/6-311++G** C-C(σ)* NBO in Vinylamine at 10 Degree Torsion

Ethanamide

Carbonyl sigma/pi separation

Ethanamide is the simplest molecule that can demonstrate the hyperconjugative interactions with the amide carbonyl group that may be seen in peptides. In parallel beta strands, the O-C-CA-HA torsion may be taken as 173 degrees and in antiparallel beta strands as -165 degrees [42], being 7 and 15 degrees respectively from perfect antiperiplanar. We denote the ethanamide non-amide carbon as CA for commonality with peptides. Given the equivalence of the hydrogens connected to CA in ethanamide, rather than refer to them as HA1, HA2 and HA3, we refer to them generically as H, referring to them by O-C-CA-H dihedral angle.

Figure 14 and Ap1:Figure 29 contrast the difference in loss sigma/pi symmetry of the carbonyl orbitals when B3LYP versus MP2 is used. The y axis scales differ markedly, for the B3LYP loss of p character is ~5% for basis sets 6-31G** and Def2SVP at 175 degrees O-C-CA-H torsion. Secondarily, for basis sets Def2TZVP, Def2TZVPP and Aug-cc-pVTZ the loss of p character approaches 1.5% at 165 degrees torsion. These data show that geometry away from perfectly antiperiplanar is necessary for hyperconjugation to disturb sigma/pi symmetry, and later figures bear out disturbances of other properties also require geometry away from perfect antiperiplanar. The 180 to 60 degree sweep of O-C-CA-H dihedrals does not quite complete the cycle of values, for only one H in CA-H is constrained, an arrangement that was selected to mimic peptide backbones in which only one of the substituents of CA is torsionally constrained. The unconstrained H that is moving into antiperiplanar dihedral angle does not remain at precisely 120 degree torsion relative to the constrained H throughout the rotation.

Hyperconjugation between the sigma carbonyl orbitals and CA-H is centered at O-C-CA-H torsion of 180 degrees, and hyperconjugation between the pi carbonyl orbitals is centered at O-C-CA-H torsion of 90 degrees. Disturbances of properties at torsional angles associated with pi carbonyl hyperconjugation can be seen Ap1:Figure 31, Ap1:Figure 32 and Ap1:Figure 34.

Figure 16 shows a reduction in Second Order Perturbative Analysis, SOPT, of donor-acceptor interactions [6] for the primary amide resonance delocalization of ~61 kcal/mol to ~41 kcal/mol in 5 degrees of torsion from antiperiplanar with B3LYP and basis set 6-31G**, and also large reduction with Def2SVP. Ap1:Figure 22 shows the N(lp) delocalization into C-O(s)* rather than C-O(p)*. However, with 6-311++G**, the variation in amide resonance delocalization throughout the range of torsion is only ~2 kcal/mol. This is a very large variation between basis sets. The relative flatness of the 6-311++G** curve, also seen in Ap1:Figure 33 in the occupancy of the C-O(pi)* NBO, suggests that with a perfect basis set B3LYP amide resonance would be calculated as invariant except near maximum sigma hyperconjugation, which then suggests B3LYP is relatively insensitive to pi hyperconjugation.

Figure 15 shows large bond bending with B3LYP and all basis sets tested, with the least being ~8 degrees (i.e. angle of ~82 degrees) with 6-311++G**. For the properties studied, this basis set often performs favourably with DFT methods. A minor cautionary note arises from Ap1:Figure 32, being that N pyramidalization increases to ~2.5 degrees rather than the ~1 degree seen for other basis sets at 100 degrees torsion which is 10 degrees from maximum pi carbonyl hyperconjugation.

Ap1:Figure 19 shows that the steric exchange energy of C-O(s) | C-O(p) increases from 0 to ~25 kcal/mol with 6-31G** in 5 degrees of O-C-CA-H torsion from antiperiplanar. Ap1:Figure 20 shows that in the same torsional range O(lp-s) | C-O(p) increases from 0 to ~7.5 kcal/mol with 6-31G**. Ap1:Figure 21 shows that in this torsional range O(lp-s) | C-O(s) decreases by ~6 kcal/mol with 6-31G**.

Pyramidalization at nitrogen

Figure 17 shows how erratic 6-311++G** is with MP2. This accords with the modern practice of using correlation consistent rather than Pople basis sets [43] with wavefunction methods. MP2/6-311++G** is greatly disturbed by correlation associated with each of sigma and pi carbonyl hyperconjugation. Figure 18 shows the loss of O-C-N-H planarity associated with this disturbance. During the rotation, planarity is lost by 15 degrees in both directions from the amide plane. Correlation associated with hyperconjugation makes sp³ pyramidalization of N more favourable than planarity, weakening the amide resonance. At 95 degrees torsion, just 5 degrees from maximum pi hyperconjugation, the dihedral describing the non-planarity changes sign, breaking the symmetry centered at 120 degrees O-C-CA-H torsion. Non-planarity is not limited to Pople basis sets. With Def2TZVP, the non-planarity is quite significant at ~7 degrees, with Def2QZVPP at ~5 and Aug-cc-pVTZ at ~3 degrees. At the hyperconjugative torsions at which amide non-planarity occurs, calculated amide resonance is impaired and necessarily so is the RAHB in which the amide might participate and hence cooperativity in hydrogen bonded secondary structures. The resonance of only one amide group in a hydrogen bonded chain need be erroneously calculated for RAHB throughout the chain to be in error. Since these errors all result in reduction of amide resonance, there are no compensating errors. Errors in the calculation of the resonance of multiple groups cooperate in producing error in the hydrogen bonding of the chain. Due to this cooperativity of errors, it is quite important that amide resonance be accurately calculated. Def2QZVPP and Aug-cc-pVTZ are of reasonable size and repute, and this pyramidalization calls into question the use of MP2 for geometry optimization of peptides/proteins. This test is suitable for benchmarking during and after development of MP2

variants. Perhaps CCSD does not fail in this manner, but optimization with CCSD with large basis sets is not yet viable for extensive studies.

The findings of pyramidalization at amide N with MP2 are similar to the non-planarity of benzene reported in [17]. Basis sets passing the benzene planarity test by having positive vibrational frequencies at planarity, such as Aug-cc-pVTZ, do not fare altogether well in the geometry optimization tests used here although the correlation consistent basis sets are constructed to provide basis set incompleteness error, BSIE, balance. The paper attributes the failures to elevated sigma-pi correlation. The paper gives that one-electron theories such as DFT are immune to this two-electron BSIE. The errors with DFT reported above are then of different origin, but will still be a result of incorrect emphasis on certain correlations. The paper points out that Atomic Natural Orbital [44, 45], ANO, basis sets are better again than correlation consistent basis sets, since ANO minimizes basis set superposition errors. We have not used ANO basis sets due to their computational expense. This pyramidalization at MP2/6-311++G** is correctable by geometry optimization on the Counterpoise Correction potential energy surface with fragment boundaries defined at the C-N bond of ethanamide, but not at the C-C bond (Ap2:Table 2).

Ap1:Figure 37 shows that the SCS correction to MP2 slightly attenuates resonance-type delocalization from the nitrogen lone pair NBO, but not in conjunction with Orbital Optimization. DLPNO-CCSD(T) single point calculation over geometry resulting MP2/Aug-cc-pVQZ is in keeping the SCS-corrected but not orbital-optimized results. This suggests suitability of SCS-MP2 optimization for DLPNO-CCSD(T) single point calculation for such studies. Since the SCS-MP2 and RI-SCS-MP2 results do not differ appreciably, RI-SCS-MP2 is useful for its reduced run-times. The DFT methods that produce results closest to those of SCS-MP2 are VSXC [46], tHCTH [47], B97D3 [27, 48] and N12 [49]. The furthest are from M11L [50], M06 [51], wB97 [52] and LC-wPBE, and these will underestimate amide resonance. As always, HF is far outlying and greatly underestimates amide resonance. Further light is cast on the irregular M11L results seen in figures Ap1:Figure 35, Ap1:Figure 36, Ap1:Figure 38 and Ap1:Figure 39 by the O-C-N-H dihedral values seen in Ap1:Figure 40 in which variation with basis set is ~20 degrees. M11L is subject to the pyramidalization at nitrogen seen with MP2. As M11L is DFT, this pyramidalization is of different origins than that with MP2. The ~13 degree pyramidalization seen with Gaussian at MP2/6-311++G** is not seen with Orca even when the NoFrozenCore option is used for greater commonality with Gaussian defaults. The Gaussian option Stable=Opt reveals that the wavefunctions for both M11L and MP2 are stable at the optimized geometry. Gaussian Stable=Opt also deems the wavefunction associated with the Orca-produced geometry to be stable. The vibrational frequencies check for geometric stability is not applicable since constraints are used. When Gaussian optimization proceeds from the Orca-optimized geometry, the highly pyramidalized geometry results. When Orca optimization proceeds from the Gaussian-optimized geometry, the highly pyramidalized geometry remains. The Orca stationary point is evidently not seen by Gaussian, though the Gaussian stationary point is seen by Orca. Developers and users of MP2 variant methods need to be aware of this variation in optimized geometry, for from it follows significant consequences for amide resonance and flexibility of protein backbones. A pyramidalization of ~13 degrees might be converted to such a pyramidalization in the other direction by backbone strain, giving a ~26 degree flexibility in each protein backbone omega (CA-C-N-CA') torsion. CASSCF [53] (8,7)/MRCI+Q[38] with Def2-TZVPP and auxiliary Def2-TZVPP/C over the MP2/6-311++G** geometry gives 0.8372 weight on a single configuration in ground state, so this pyramidalized geometry is only weakly associated with multireference character. Table 1 gives the results of this multireference method for the non-pyramidalized geometries arising from beta strand psi torsions with MP2/Aug-cc-pVQZ, showing very good agreement with single reference wavefunction methods, and that the problem is not particularly multireference.

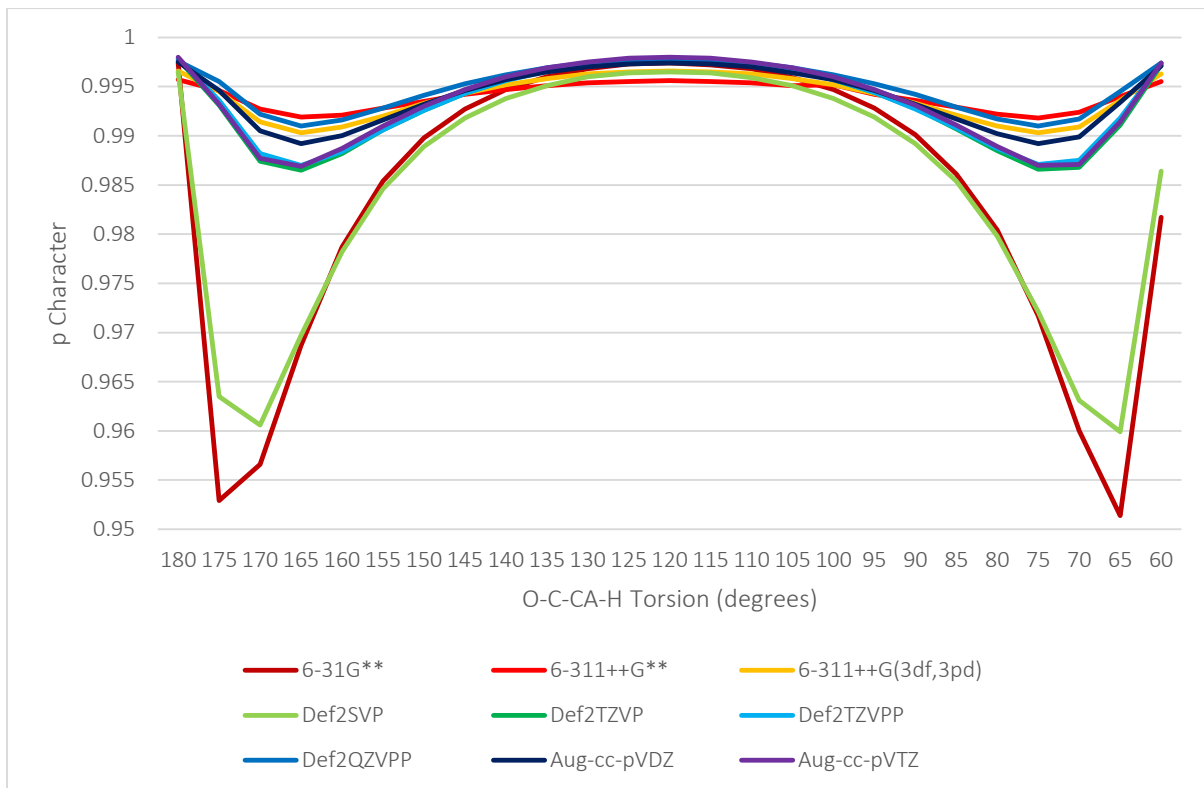


Figure 14. $C\text{-}O(\pi)$ Carbon NHO p Character in Ethanamide at Varying O-C-CA-H Torsion and Basis Set at B3LYP

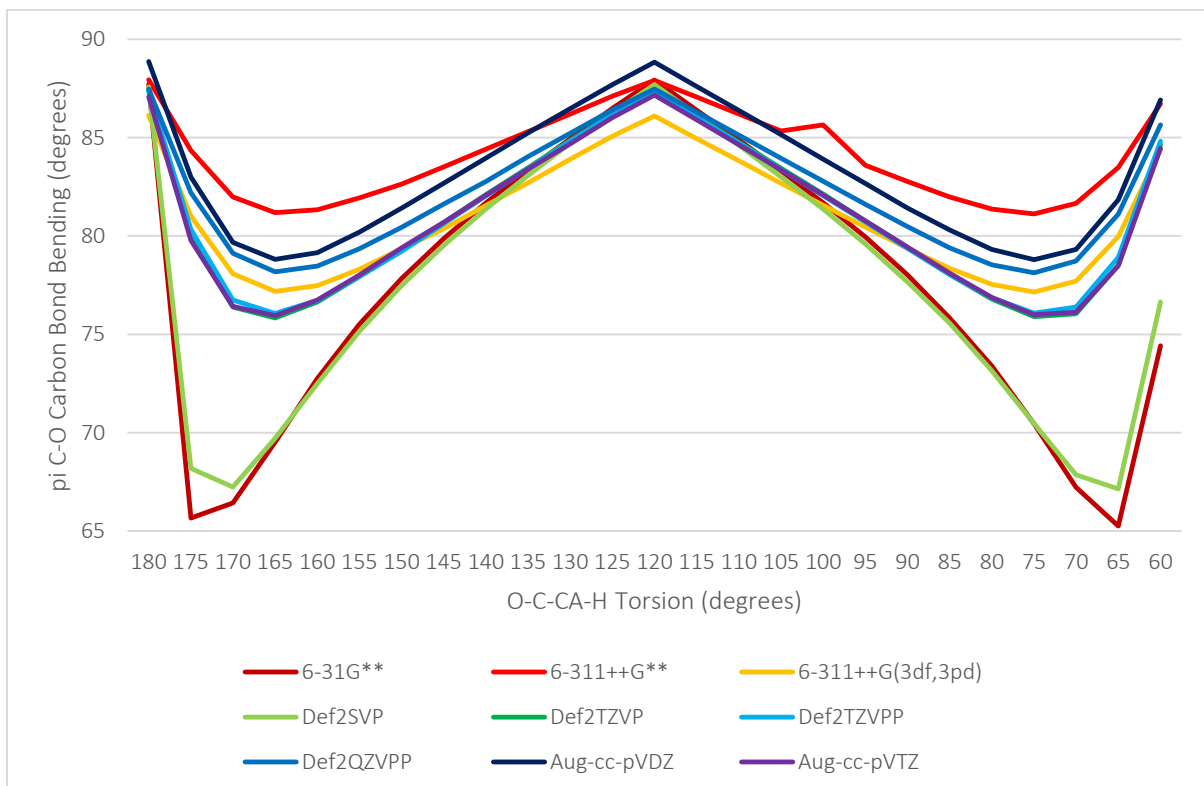


Figure 15. $C\text{-}O(\pi)$ Carbon NHO Bond Bending in Ethanamide at Varying O-C-CA-H Torsion and Basis Set at B3LYP

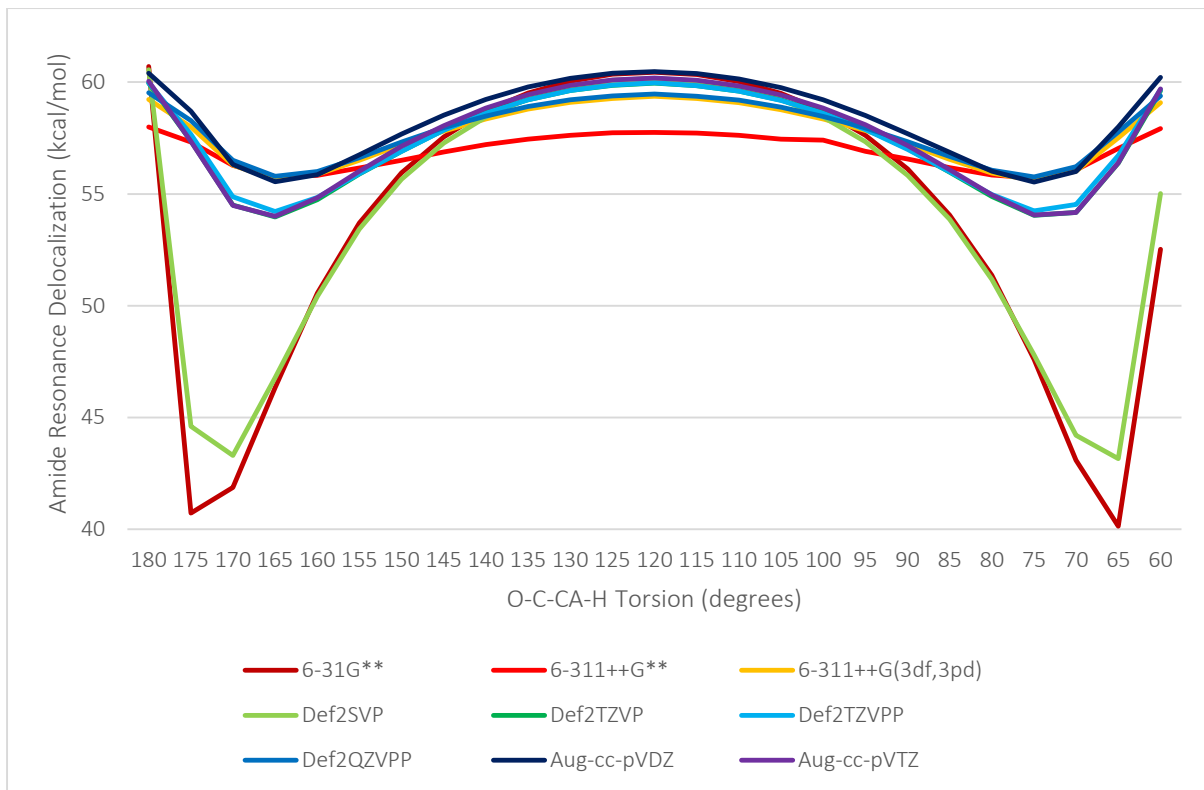


Figure 16. Second Order Perturbation Theory Primary Amide Resonance Delocalization ($N(lp) \rightarrow C-O(pi)^*$) in Ethanamide at Varying O-C-CA-H Torsion and Basis Set at B3LYP

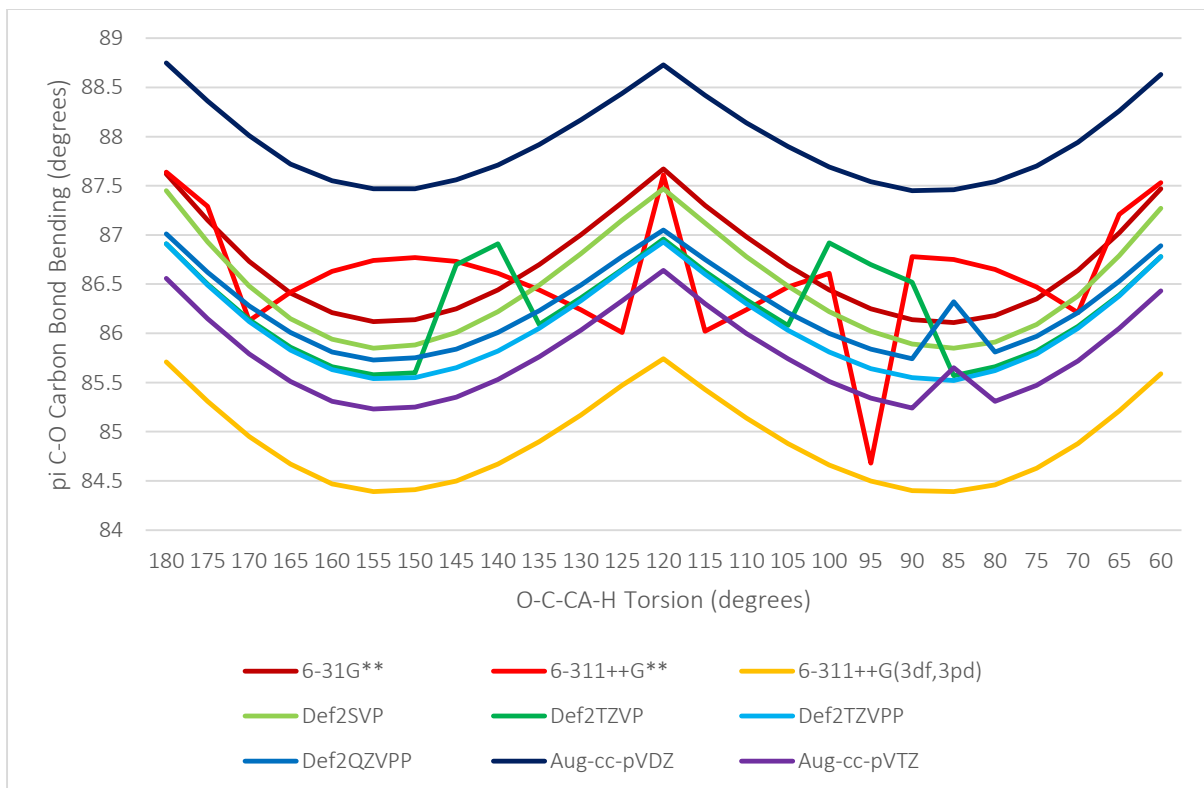


Figure 17. C-O(pi) Carbon NHO Bond Bending in Ethanamide at Varying O-C-CA-H Torsion and Basis Set at MP2

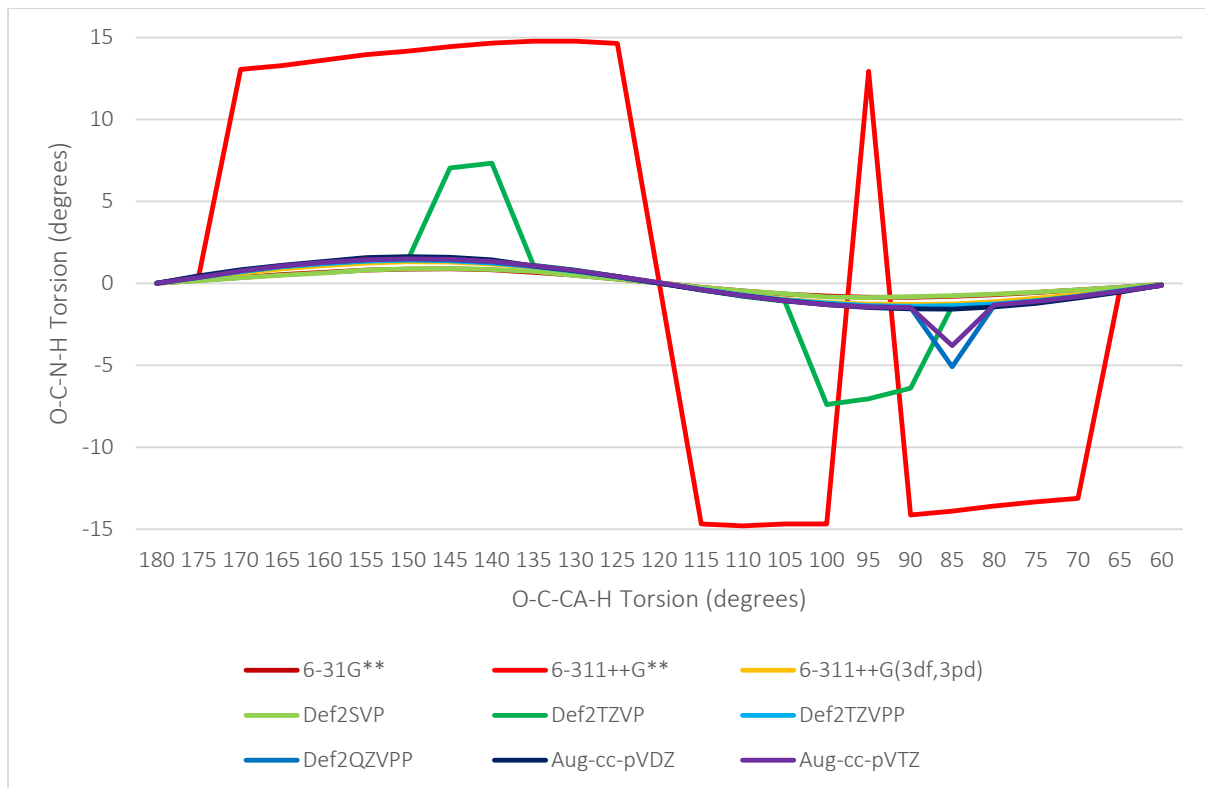


Figure 18. O-C-N-H Torsion in Ethanamide with Varying O-C-CA-H Torsion and Basis Set at MP2

Antiparallel beta sheet

Ap2:Table 3 and Ap2:Table 4 refer to gas phase antiparallel beta sheets which have been geometry optimized with TeraChem 1.5K at LC-wPBE (keyword wpbe in TeraChem) omega 0.4 and 6-31G**. While the ethanamide model requires optimization constraints to demonstrate hyperconjugation, these beta sheet require no constraints, that is, they are fully optimized. Ap2:Table 3 refers to a polyvaline structure and Ap2:Table 4 to a polyalanine structure.

By extending ethanamide to species resembling alanine and valine, it can be shown that these backbone errors are very sensitive to sidechain even for uncharged and non-polar residues, so that the utility of methods afflicted of these errors is dubious in the case of heterogeneous amino acid residues. Also, it might be erroneously concluded that this modulation of backbone amide resonance by sidechain is a means by which sidechain determines protein fold.

The variation in the N(lp)->C-O(pi)* SOPT (“SoptP” column) has two sources, one being RAHB which tends to cause amide resonance in hydrogen bonded amide chain to peak in the middle of the chain and be lowest at the ends, and the effects being discussed here, bond bending and loss of local symmetry. These tables make the point that this bond bending and loss of local symmetry exists in beta sheet rather than just the ethanamide model.

These tables are sorted on bond bending (“Dev” column). While bond bending might be expected to be dependent of d orbital involvement to give non-cylindrically symmetric orbitals so the hybrids can point at each other, these tables, particularly Ap2:Table 3, do not strongly bear out this notion.

SOPT kcal/mol values under 1.0 do not appear in these tables. Noteworthy are the variations in $N(\text{lp}) \rightarrow C-\text{O}(\text{p})^*$ SOPT ("SoptP") and $N(\text{lp}) \rightarrow C-\text{O}(\text{s})^*$ SOPT ("SoptS"). That the latter is non-zero is evidence of carbonyl orbital disturbance.

There is a strong but imperfect association between the occupancy of $C-\text{O}(\text{s})^*$ and bond bending and loss of carbonyl sigma/pi symmetry. Perhaps non-double hybrid DFT methods do not deal well with the situation in which there is occupancy of $C-\text{O}(\text{s})^*$ in the context of large occupancy of the $C-\text{O}(\text{p})^*$.

In Ap2:Table 4, the least bond bending is associated with O-C-CA-HA dihedral of ~ 150 degrees, which corresponds to the optimal angle (90 degrees) for hyperconjugation involving $C-\text{O}(\text{p})^*$ orbitals. This suggests that this hyperconjugation is not disruptive as hyperconjugation involving $C-\text{O}(\text{s})^*$.

Moderate SOPT kcal/mol values are proportional to resonance-type charge transfer [6]. The difference between hyperconjugative charge transfer from the methyl group into $C-\text{O}(\text{p})^*$ and $C-\text{O}(\text{s})^*$ has some association with bond bending and loss of sigma/pi symmetry. The variation in individual and collective hyperconjugative SOPT values is less than that of amide resonance, suggestive of a failure of method.

Conclusion

In contrast to single and multireference wavefunction methods, in the molecules studied, established DFT methods do not substantially maintain sigma/pi separation or bond straightness in double bonds that have hyperconjugative interactions at other than perfect antiperiplanar geometry. Unlike ethene with C-C torsion, these failures are not due to the problem being multireference. The double hybrid DFT methods are considerably better than other DFT methods, but do not quite attain the accuracy of MP2 methods though they incur similar computational costs. This DFT error is encountered in study of proteins which include parallel and antiparallel beta sheet and attenuates amide resonance and hence necessarily RAHB in the hydrogen bonded chains of backbone amides. Since RAHB is cooperative, if all errors in calculations of amide resonance give values that are lower than accurate, then the errors themselves may be seen as cooperative. Since every backbone amide in a beta sheet is subject to roughly the same torsional hyperconjugation, beta sheet hydrogen bonding is cooperatively reduced. While the smaller basis sets such as D95** [54], 6-31G** and Def2SVP [55] are associated with the largest reductions in amide resonance, these basis sets have been popular because they are the largest that could be used at the atom count of beta sheets. Great caution is needed in interpreting the results of applying established DFT methods to proteins.

While this work focusses on amide resonance and RAHB, any non-double hybrid DFT calculated amide property is at risk of being significantly inaccurate due to this error. A range of quantities is disturbed by this error along with carbonyl sigma/pi separation and bond straightness, including charge transfers $N(\text{lp}) \rightarrow C-\text{O}(\text{p})^*$ and $N(\text{lp}) \rightarrow C-\text{O}(\text{s})^*$ and steric interactions $C-\text{O}(\text{p}) \mid C-\text{O}(\text{s})$, $O(\text{lp-s}) \mid C-\text{O}(\text{p})$ and $O(\text{lp-s}) \mid C-\text{O}(\text{s})$.

It can be shown with molecular species extending ethanamide to approximate alanine and valine that the loss of local symmetry with DFT is very sensitive to residue type. With heterogeneous amino-acid beta sheet, DFT geometry optimization will be erratic rather than reliably wrong. Also, this sensitivity invites the erroneous conclusion that protein folding is influenced by this sidechain modulation of backbone amide resonance.

MP2 has a basis set and optimization implementation dependent propensity for large variation in pyramidalization at the amide nitrogen in ethanamide at C-CA torsion. This pyramidalization necessarily competes with amide resonance. When the tendency to pyramidalize becomes dominant, calculation will under-estimate RAHB for hydrogen bonded chains in which the amide is potentially

involved. Also, the flexibility of a protein backbone is incorrectly increased since the pyramidalization may be switched from one side to another by backbone strain, giving large backbone amide omega torsion. This variation is not limited to Pople basis sets, and is seen at lesser extent and in small ranges of C-CA torsion with Def2TZVP, Def2QZVPP and Aug-cc-pVTZ. This is not exclusively an MP2 issue, for the quite recent DFT method M11L also demonstrates this pyramidalization at antiparallel beta strand psi torsion with most basis sets tested. This pyramidalization error is not unambiguously present in geometry-optimized protein coordinates since this pyramidalization may arise by other means such as backbone strain and hydrogen bonding, so validation of methods with respect to this error is best done on small amides such as ethanamide or N-methylethanamide. In ethanamide, this second problem can be corrected by geometry optimization on the Counterpoise Corrected potential energy surface by definition of fragment boundaries at the C-N bond, but not at the C-C bond.

We recommend that non-wavefunction electronic structure calculation of protein be accompanied by NBO analysis of backbone amide carbonyl local symmetry and bond bending. Since hyperconjugations involving C-O(s)* and C-O(p)* are available at various C-CA torsions, this recommendation extends beyond the secondary structure tested here, antiparallel beta sheet, to other protein secondary structure types that have hydrogen bonded chains of backbone amides. While the consequences of inaccurate calculation amide resonance are not amplified in random coil as in secondary structure, they may be expected to be significant in determining random coil structure and hydrogen bonding networks.

NBO-based assessment of maintenance of local symmetry and bond bending is proposed for evaluation of existing or development of new electronic structure system methods. The tests used here involving vinylamine and ethanamide could serve as standard benchmarks. Measurement of pyramidalization and NBO assessment of sp hybridization at the amide nitrogen in ethanamide with carbonyl hyperconjugation at torsion could similarly serve as a standard benchmark.

Acknowledgements

Thanks to Peter M. W. Gill for pointing out the resemblance of the second mentioned problem, pyramidalization at amide nitrogen at wavefunction method/Pople basis set, to the benzene non-planarity problem [17].

Thanks to eResearch South Australia for hosting and administering machines provided under Australian Government Linkage, Infrastructure, Equipment and Facilities grants for Supercomputing in South Australia, and for allocating 64 CPU cores and 256 GB RAM of the NeCTAR Research Cloud (a collaborative Australian research platform supported by the National Collaborative Research Infrastructure Strategy) to the present work, without which the present work would not have been possible.

References

1. Bertolasi, V., et al., *Evidence for resonance-assisted hydrogen bonding. 2. Intercorrelation between crystal structure and spectroscopic parameters in eight intramolecularly hydrogen bonded 1,3-diaryl-1,3-propanedione enols*. Journal of the American Chemical Society, 1991. **113**(13): p. 4917-4925.
2. Bertolasi, V., et al., *Intermolecular N–H···O hydrogen bonds assisted by resonance. Heteroconjugated systems as hydrogen-bond-strengthening functional groups*. Acta Crystallographica Section B, 1995. **51**(6): p. 1004-1015.
3. Bertolasi, V., et al., *pi-Bond cooperativity and anticooperativity effects in resonance-assisted hydrogen bonds (RAHBs)*. Acta Crystallogr B, 2006. **62**(Pt 5): p. 850-63.

4. Pauling, L. and R.B. Corey, *The Pleated Sheet, A New Layer Configuration of Polypeptide Chains*. Proceedings of the National Academy of Sciences, 1951. **37**(5): p. 251-256.
5. Pauling, L., R.B. Corey, and H.R. Branson, *The structure of proteins: Two hydrogen-bonded helical configurations of the polypeptide chain*. Proceedings of the National Academy of Sciences, 1951. **37**(4): p. 205-211.
6. Weinhold, F.A. and C.R. Landis, *Valency and Bonding: A Natural Bond Orbital Donor-Acceptor Perspective*. 2005: Cambridge University Press.
7. Weinhold, F. and C.R. Landis, *Discovering Chemistry with Natural Bond Orbitals*. 2012: Wiley.
8. Glendening, E.D., C.R. Landis, and F. Weinhold, *NBO 6.0: Natural bond orbital analysis program*. Journal of Computational Chemistry, 2013. **34**(16): p. 1429-1437.
9. Burke, K., *Perspective on density functional theory*. The Journal of Chemical Physics, 2012. **136**(15): p. 150901.
10. Becke, A.D., *Perspective: Fifty years of density-functional theory in chemical physics*. The Journal of Chemical Physics, 2014. **140**(18): p. 18A301.
11. Clauss, A.D., et al., *Rabbit ears concepts of water lone pairs: a reply to comments of Hiberty, Danovich, and Shaik*. Chemistry Education Research and Practice, 2015.
12. Moeller, C. and M.S. Plesset, *Note on an approximation treatment for many-electron systems*. Phys. Rev., 1934. **46**: p. 0618-22.
13. Dunning, T.H., *Gaussian basis sets for use in correlated molecular calculations. I. The atoms boron through neon and hydrogen*. The Journal of Chemical Physics, 1989. **90**(2): p. 1007-1023.
14. Grimme, S., *Semiempirical hybrid density functional with perturbative second-order correlation*. The Journal of Chemical Physics, 2006. **124**(3): p. 034108.
15. Zhao, Y., B.J. Lynch, and D.G. Truhlar, *Doubly Hybrid Meta DFT: New Multi-Coefficient Correlation and Density Functional Methods for Thermochemistry and Thermochemical Kinetics*. The Journal of Physical Chemistry A, 2004. **108**(21): p. 4786-4791.
16. Vydrov, O.A. and G.E. Scuseria, *Assessment of a long-range corrected hybrid functional*. The Journal of Chemical Physics, 2006. **125**(23): p. 234109.
17. Moran, D., et al., *Popular Theoretical Methods Predict Benzene and Arenes To Be Nonplanar*. Journal of the American Chemical Society, 2006. **128**(29): p. 9342-9343.
18. Boys, S.F. and F. Bernardi, *The calculation of small molecular interactions by the differences of separate total energies. Some procedures with reduced errors*. Molecular Physics, 1970. **19**(4): p. 553-566.
19. Gupta, A. and R.J. Boyd, *Density difference representation of electron correlation*. The Journal of Chemical Physics, 1978. **68**(4): p. 1951-1957.
20. Frisch, M.J., et al., *Gaussian 09*. 2009, Gaussian, Inc.: Wallingford, CT, USA.
21. Neese, F., *The ORCA program system*. Wiley Interdisciplinary Reviews: Computational Molecular Science, 2012. **2**(1): p. 73-78.
22. Kossmann, S. and F. Neese, *Efficient Structure Optimization with Second-Order Many-Body Perturbation Theory: The RIJCOSX-MP2 Method*. Journal of Chemical Theory and Computation, 2010. **6**(8): p. 2325-2338.
23. Ripplinger, C. and F. Neese, *An efficient and near linear scaling pair natural orbital based local coupled cluster method*. The Journal of Chemical Physics, 2013. **138**(3): p. 034106.
24. Ufimtsev, I.S. and T.J. Martinez, *Quantum Chemistry on Graphical Processing Units. 3. Analytical Energy Gradients, Geometry Optimization, and First Principles Molecular Dynamics*. Journal of Chemical Theory and Computation, 2009. **5**(10): p. 2619-2628.
25. Kästner, J., et al., *DL-FIND: An Open-Source Geometry Optimizer for Atomistic Simulations*. The Journal of Physical Chemistry A, 2009. **113**(43): p. 11856-11865.
26. Grimme, S., et al., *A consistent and accurate ab initio parametrization of density functional dispersion correction (DFT-D) for the 94 elements H-Pu*. The Journal of Chemical Physics, 2010. **132**(15): p. 154104.

27. Grimme, S., S. Ehrlich, and L. Goerigk, *Effect of the damping function in dispersion corrected density functional theory*. Journal of Computational Chemistry, 2011. **32**(7): p. 1456-1465.

28. Glendening, E.D., et al., *NBO 6.0*. 2013, Theoretical Chemistry Institute, University of Wisconsin, Madison.

29. W3C, *Extensible Markup Language (XML)*.

30. W3C, *XQuery 3.0: An XML Query Language*. 2014.

31. W3C, *XSL Transformations (XSLT) Version 3.0*. 2014.

32. *Saxon-PE*. 2015, Saxonica.

33. *Excel*. 2013, Microsoft.

34. *Jmol: an open-source Java viewer for chemical structures in 3D*.

35. Becke, A.D., *Density-functional thermochemistry. III. The role of exact exchange*. The Journal of Chemical Physics, 1993. **98**(7): p. 5648-5652.

36. Grimme, S., *Improved second-order Møller–Plesset perturbation theory by separate scaling of parallel- and antiparallel-spin pair correlation energies*. The Journal of Chemical Physics, 2003. **118**(20): p. 9095-9102.

37. Neese, F., et al., *Assessment of Orbital-Optimized, Spin-Component Scaled Second-Order Many-Body Perturbation Theory for Thermochemistry and Kinetics*. Journal of Chemical Theory and Computation, 2009. **5**(11): p. 3060-3073.

38. Meissner, L., *Size-consistency corrections for configuration interaction calculations*. Chemical Physics Letters, 1988. **146**(3–4): p. 204-210.

39. Iikura, H., et al., *A long-range correction scheme for generalized-gradient-approximation exchange functionals*. The Journal of Chemical Physics, 2001. **115**(8): p. 3540-3544.

40. Becke, A.D., *Real-space post-Hartree–Fock correlation models*. The Journal of Chemical Physics, 2005. **122**(6): p. 064101.

41. Scuseria, G.E., C.L. Janssen, and H.F. Schaefer, *An efficient reformulation of the closed-shell coupled cluster single and double excitation (CCSD) equations*. The Journal of Chemical Physics, 1988. **89**(12): p. 7382-7387.

42. Pettersen, E.F., et al., *UCSF Chimera—A visualization system for exploratory research and analysis*. Journal of Computational Chemistry, 2004. **25**(13): p. 1605-1612.

43. Ditchfield, R., W.J. Hehre, and J.A. Pople, *Self-Consistent Molecular-Orbital Methods. IX. An Extended Gaussian-Type Basis for Molecular-Orbital Studies of Organic Molecules*. The Journal of Chemical Physics, 1971. **54**(2): p. 724-728.

44. Martin, J.M.L., P.R. Taylor, and T.J. Lee, *The harmonic frequencies of benzene. A case for atomic natural orbital basis sets*. Chemical Physics Letters, 1997. **275**(3–4): p. 414-422.

45. Martin, J.M.L., T.J. Lee, and P.R. Taylor, *A purely ab initio spectroscopic quality quartic force field for acetylene*. The Journal of Chemical Physics, 1998. **108**(2): p. 676-691.

46. Van Voorhis, T. and G.E. Scuseria, *A novel form for the exchange-correlation energy functional*. The Journal of Chemical Physics, 1998. **109**(2): p. 400-410.

47. Boese, A.D. and N.C. Handy, *New exchange-correlation density functionals: The role of the kinetic-energy density*. The Journal of Chemical Physics, 2002. **116**(22): p. 9559-9569.

48. Grimme, S., *Semiempirical GGA-type density functional constructed with a long-range dispersion correction*. Journal of Computational Chemistry, 2006. **27**(15): p. 1787-1799.

49. Peverati, R. and D.G. Truhlar, *Exchange–Correlation Functional with Good Accuracy for Both Structural and Energetic Properties while Depending Only on the Density and Its Gradient*. Journal of Chemical Theory and Computation, 2012. **8**(7): p. 2310-2319.

50. Peverati, R. and D.G. Truhlar, *M11-L: A Local Density Functional That Provides Improved Accuracy for Electronic Structure Calculations in Chemistry and Physics*. The Journal of Physical Chemistry Letters, 2012. **3**(1): p. 117-124.

51. Zhao, Y. and D. Truhlar, *The M06 suite of density functionals for main group thermochemistry, thermochemical kinetics, noncovalent interactions, excited states, and transition elements*:

two new functionals and systematic testing of four M06-class functionals and 12 other functionals. Theoretical Chemistry Accounts, 2008. **120**(1-3): p. 215-241.

52. Chai, J.-D. and M. Head-Gordon, *Systematic optimization of long-range corrected hybrid density functionals.* The Journal of Chemical Physics, 2008. **128**(8): p. 084106.

53. Hegarty, D. and M.A. Robb, *Application of Unitary Group-Methods to Configuration-Interaction Calculations.* Molecular Physics, 1979. **38**(6): p. 1795-1812.

54. Dunning, T.H. and P.J. Hay, *Modern Theoretical Chemistry.* Vol. 3. 1977, New York: Plenum.

55. Weigend, F. and R. Ahlrichs, *Balanced basis sets of split valence, triple zeta valence and quadruple zeta valence quality for H to Rn: Design and assessment of accuracy.* Physical Chemistry Chemical Physics, 2005. **7**(18): p. 3297-3305.

Appendix 1

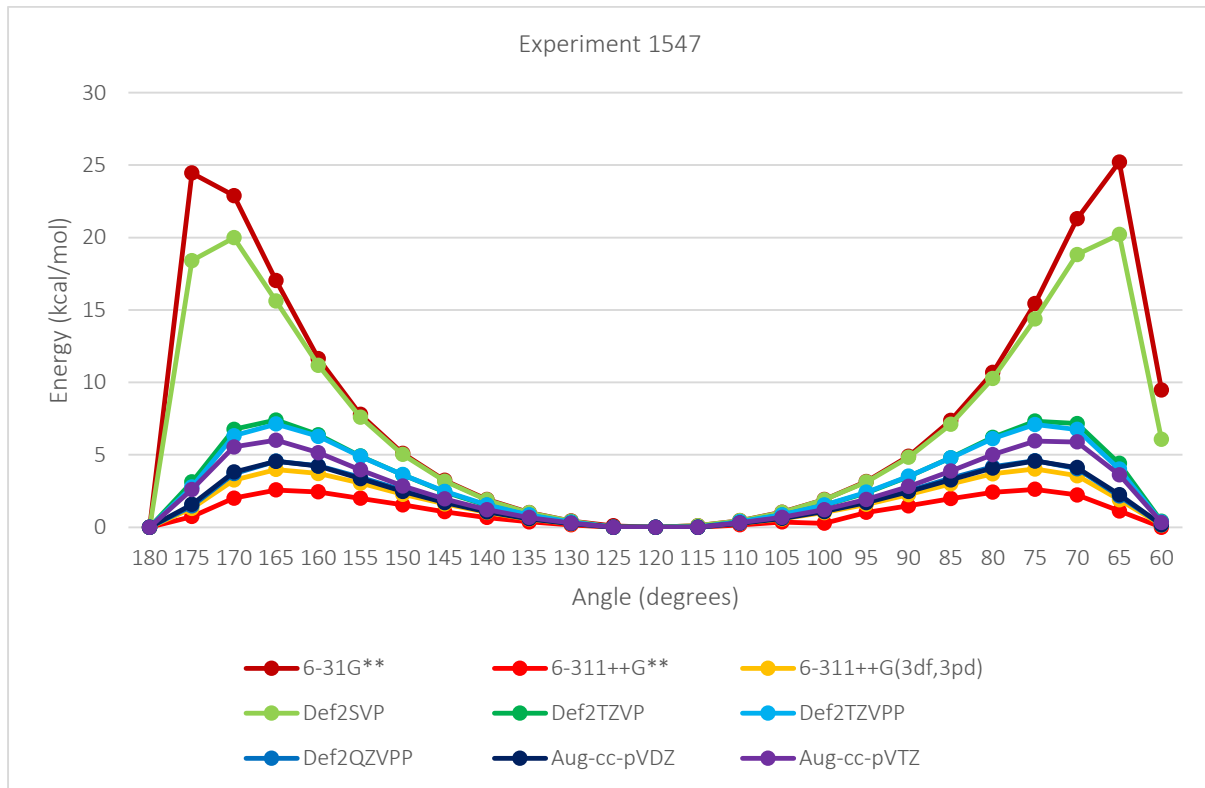


Figure 19. C-O(p)/C-O(s) Steric Exchange Energy in Ethanamide at O-C-CA-H Dihedral Angle with B3LYP

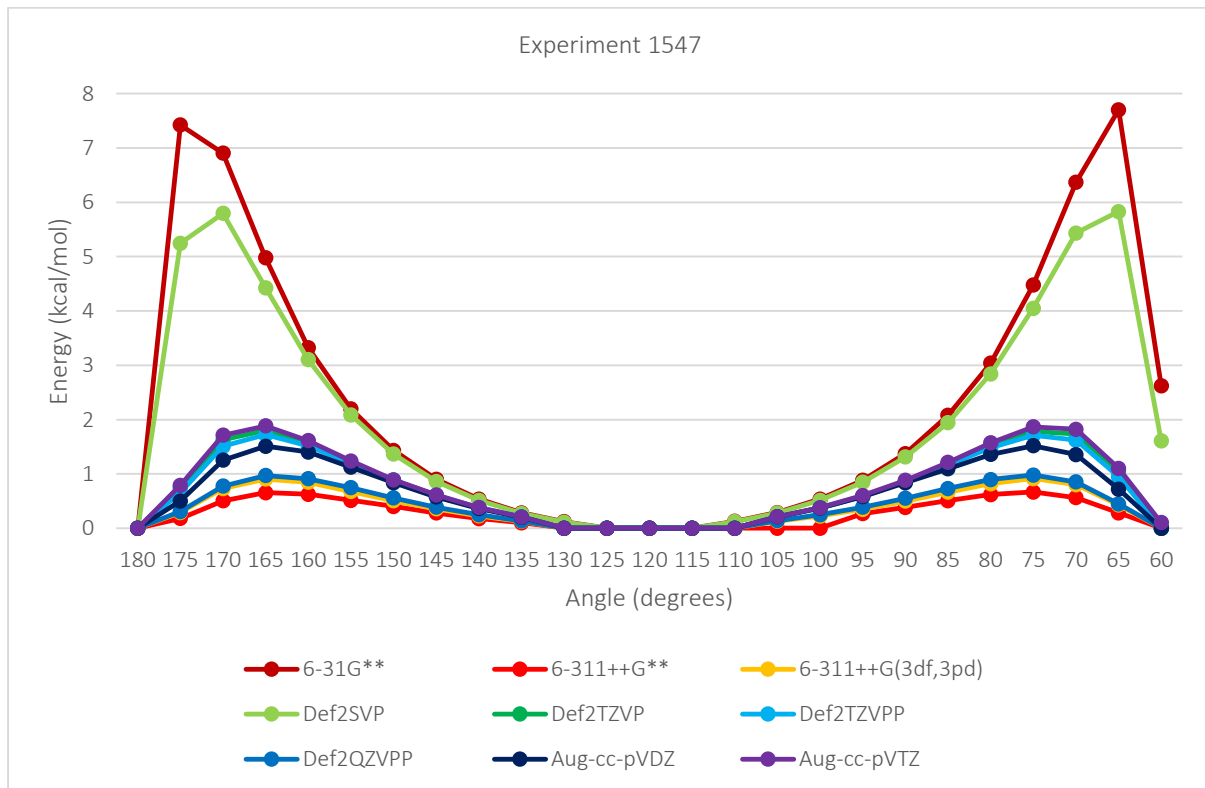


Figure 20. O(lp-s)/C-O(p) Steric Exchange Energy in Ethanamide at O-C-CA-H Dihedral Angle with B3LYP

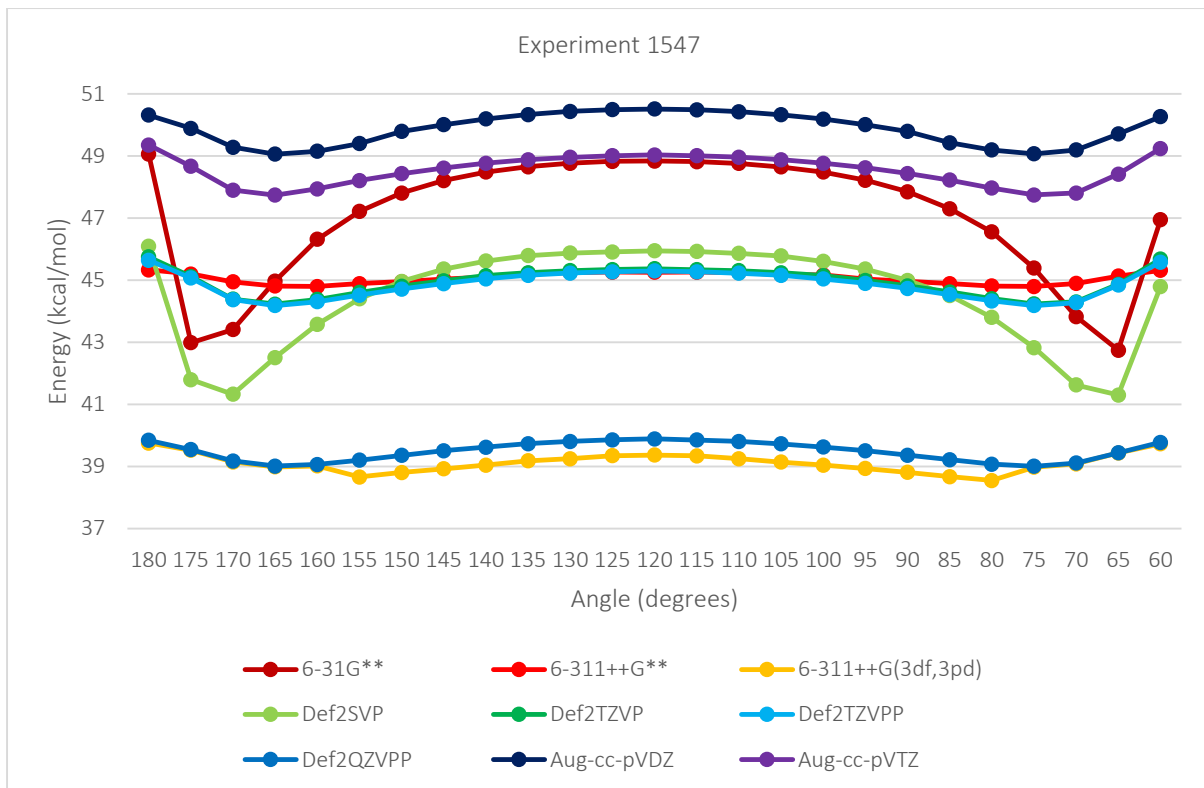


Figure 21. $O(lp-s)/C-O(s)$ Steric Exchange Energy in Ethanamide at $O-C-CA-H$ Dihedral Angle with B3LYP

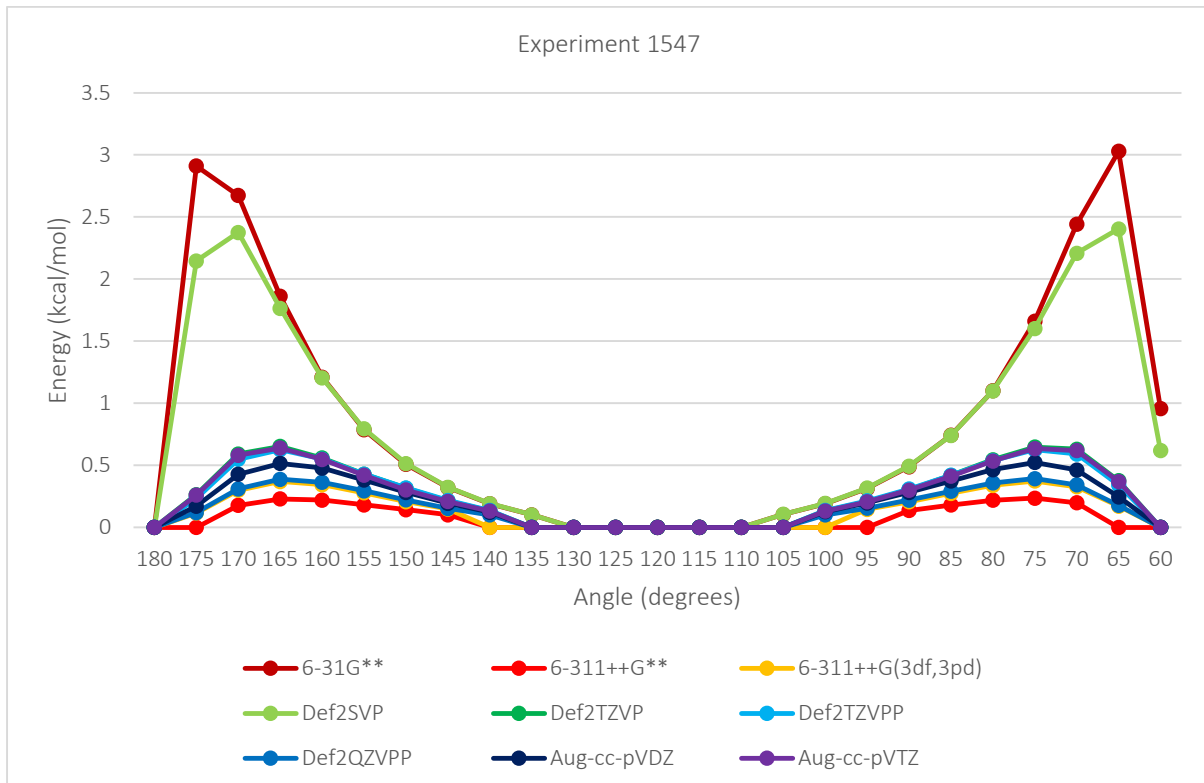


Figure 22. $N(lp)->C-O(s)^*$ SOPT Energy in Ethanamide at $O-C-CA-H$ Dihedral Angle with B3LYP. Values less than 0.01 as zero.

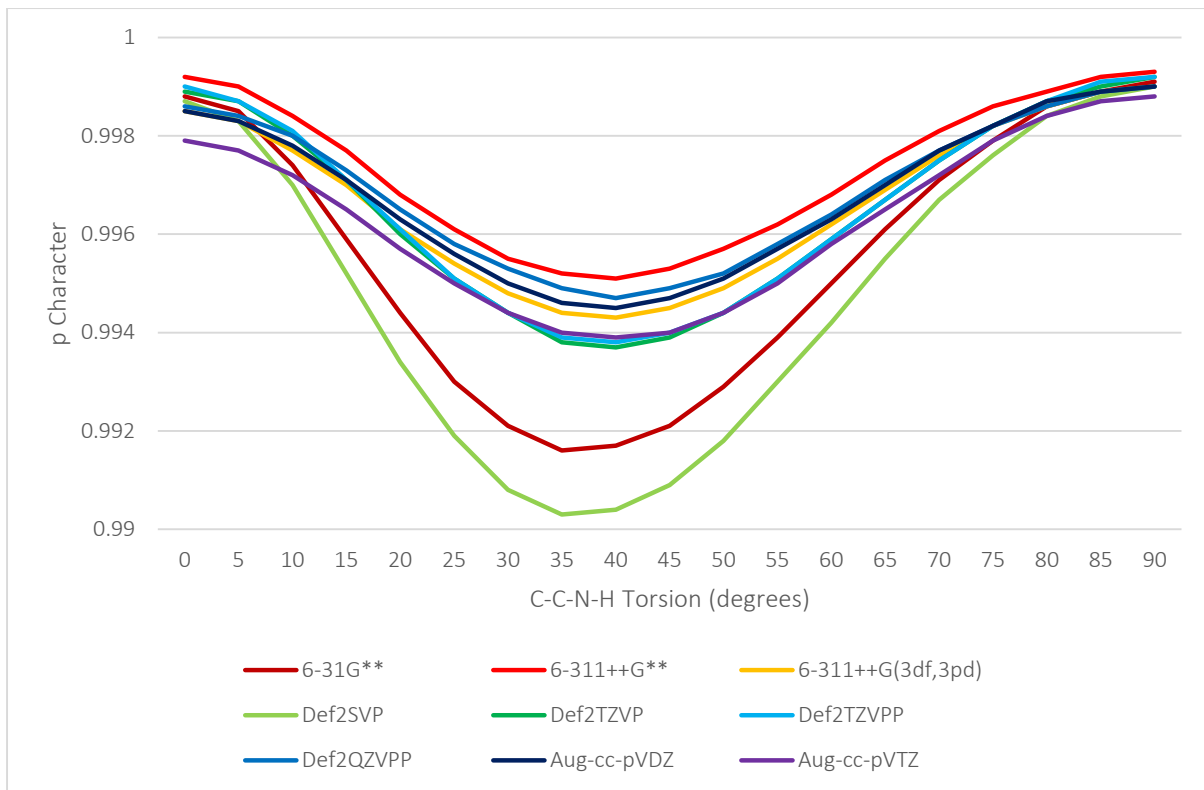


Figure 23. C-C(pi) Central Carbon NHO *p* Character in Vinylamine at Varying C-C-N-H Torsion and Basis Set at MP2

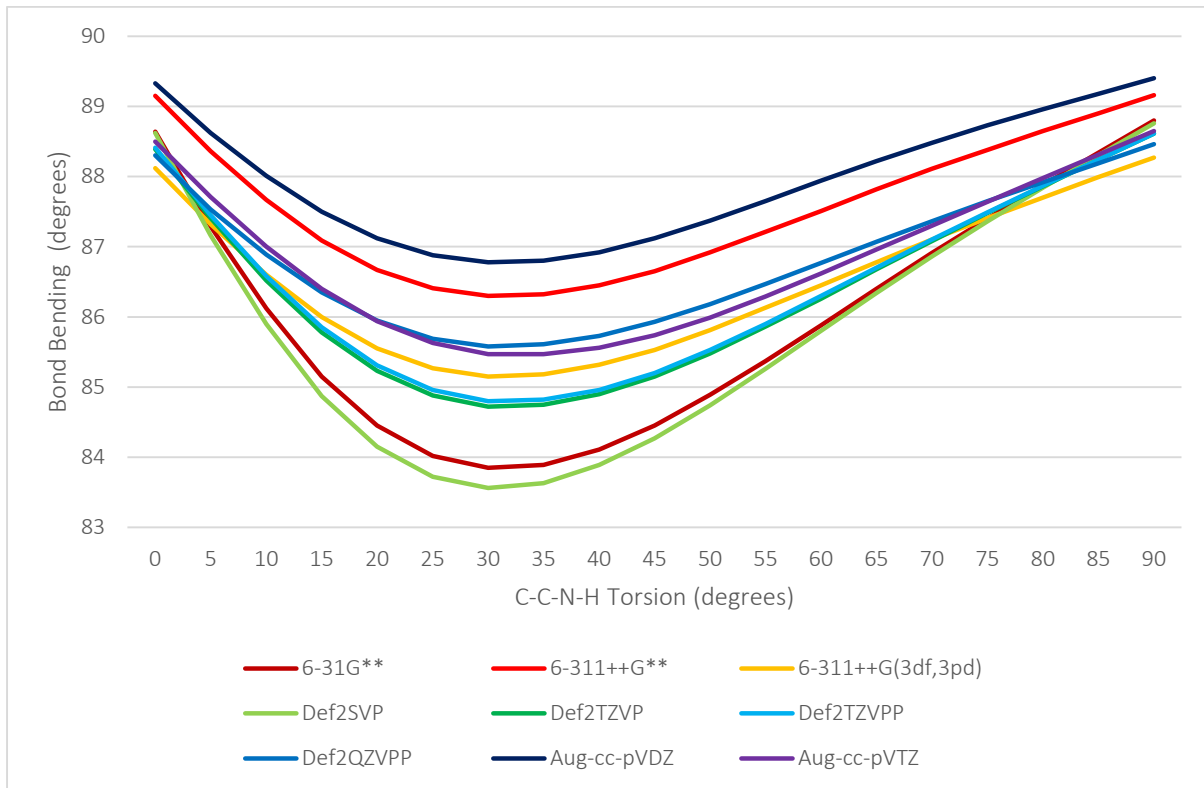


Figure 24. C-C(pi) Central Carbon NHO Bond Bending in Vinylamine at Varying C-C-N-H Torsion and Basis Set at MP2

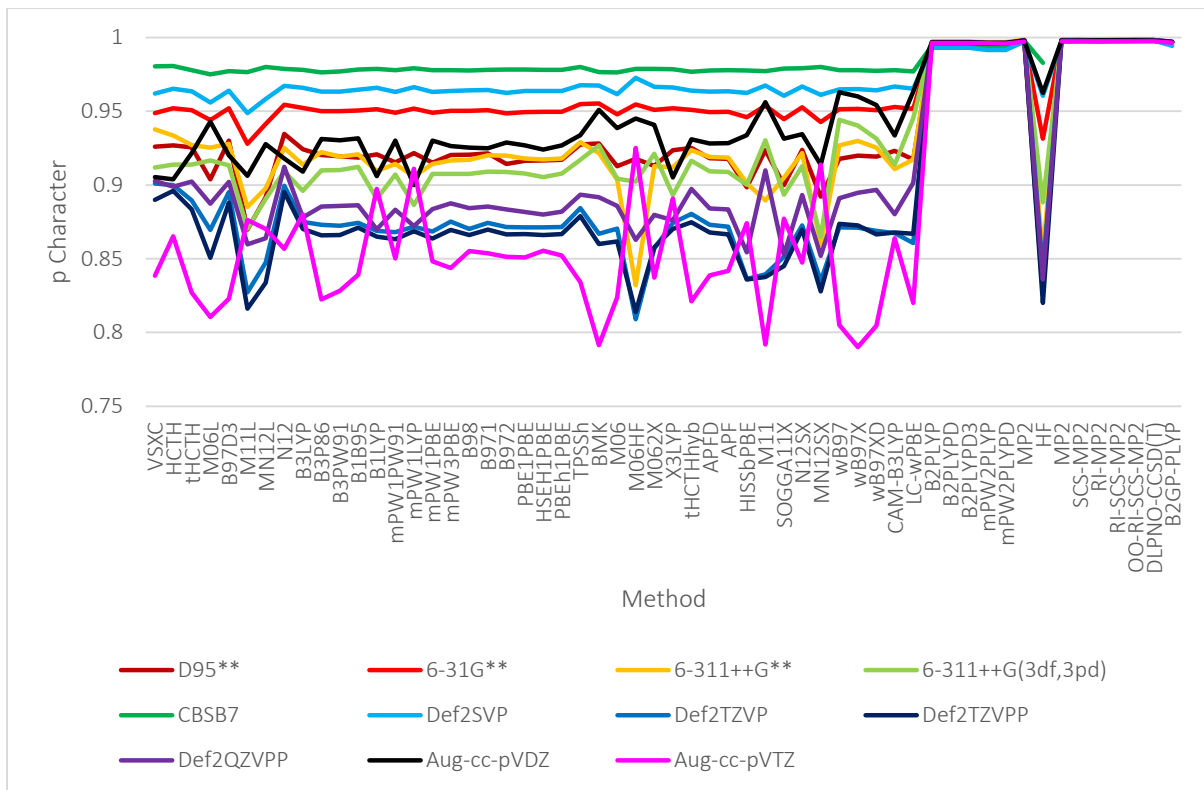


Figure 25. C-C(pi) Central Carbon NHO *p* Character in Vinylamine at 10 Degree C-C-N-H Torsion with Varying Method and Basis Set

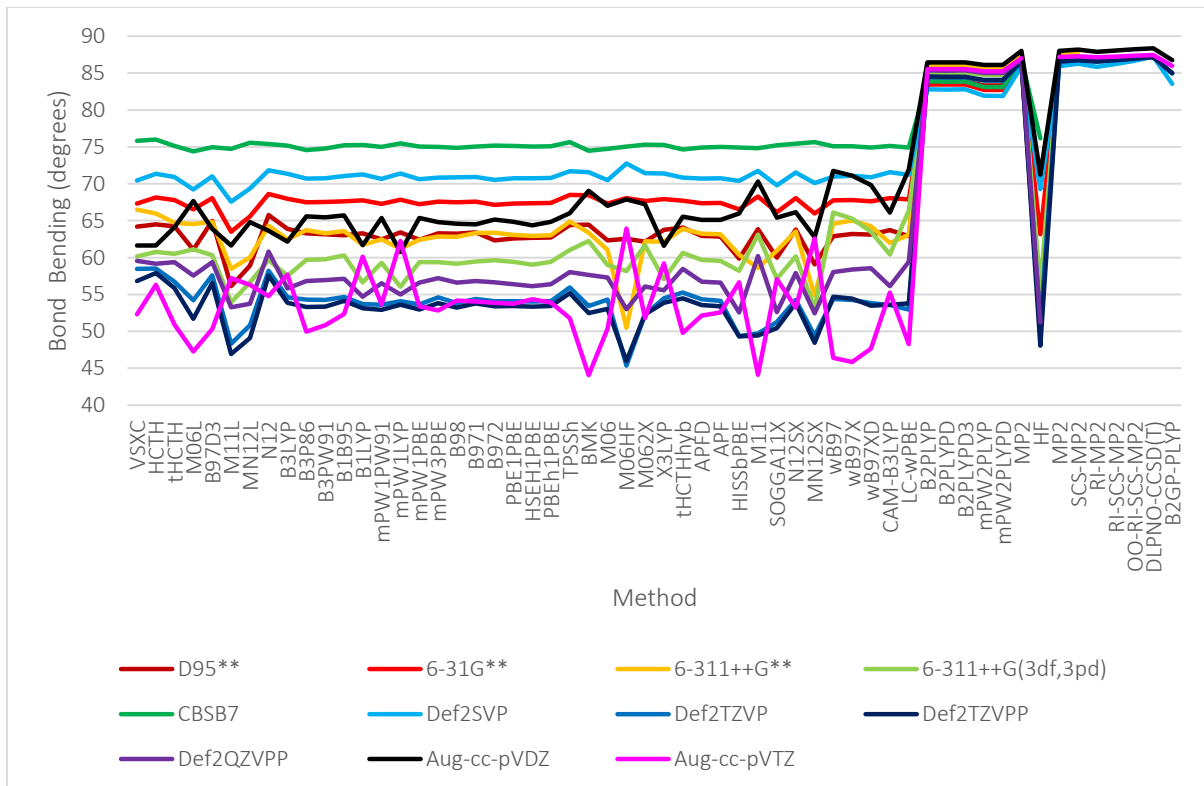


Figure 26. C-C(pi) Central Carbon NHO Bond Bending in Vinylamine at 10 degree C-C-N-H Torsion with Varying Method and Basis Set

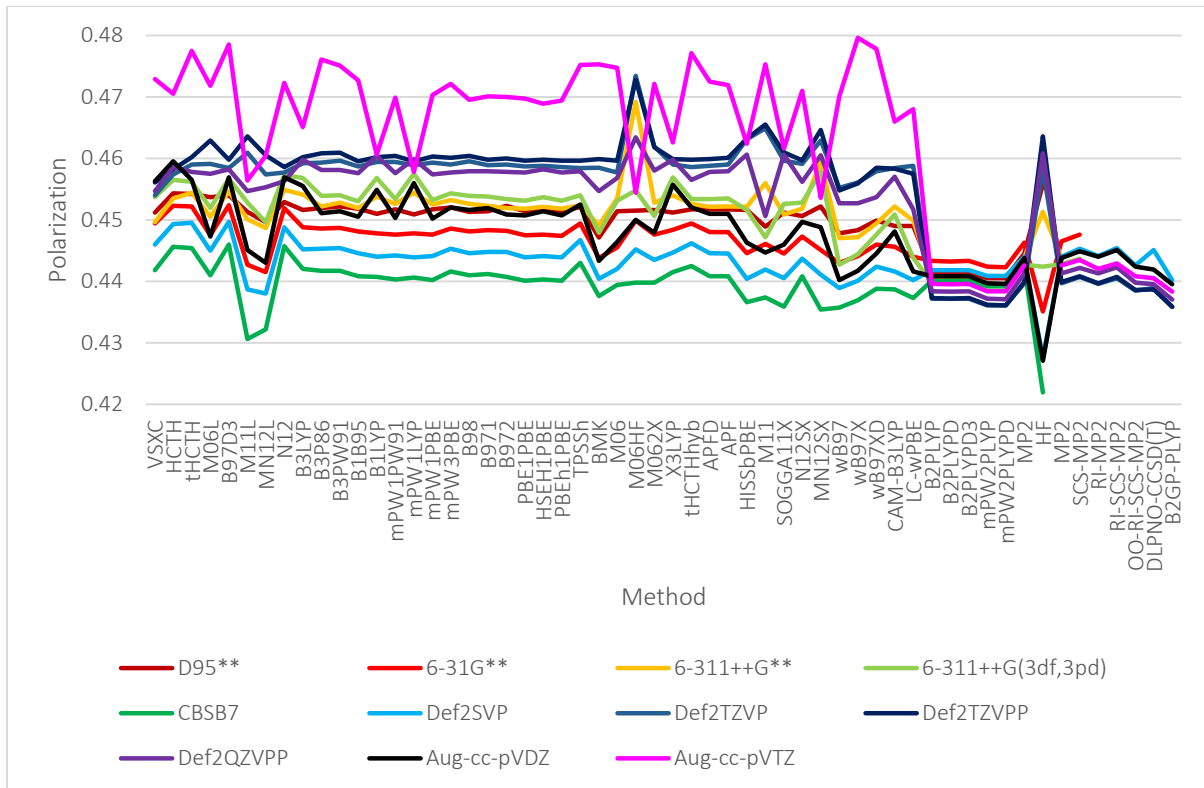


Figure 27. C-C(π) Central Carbon NHO Polarization in Vinylamine at 10 degree C-C-N-H Torsion with Varying Method and Basis Set

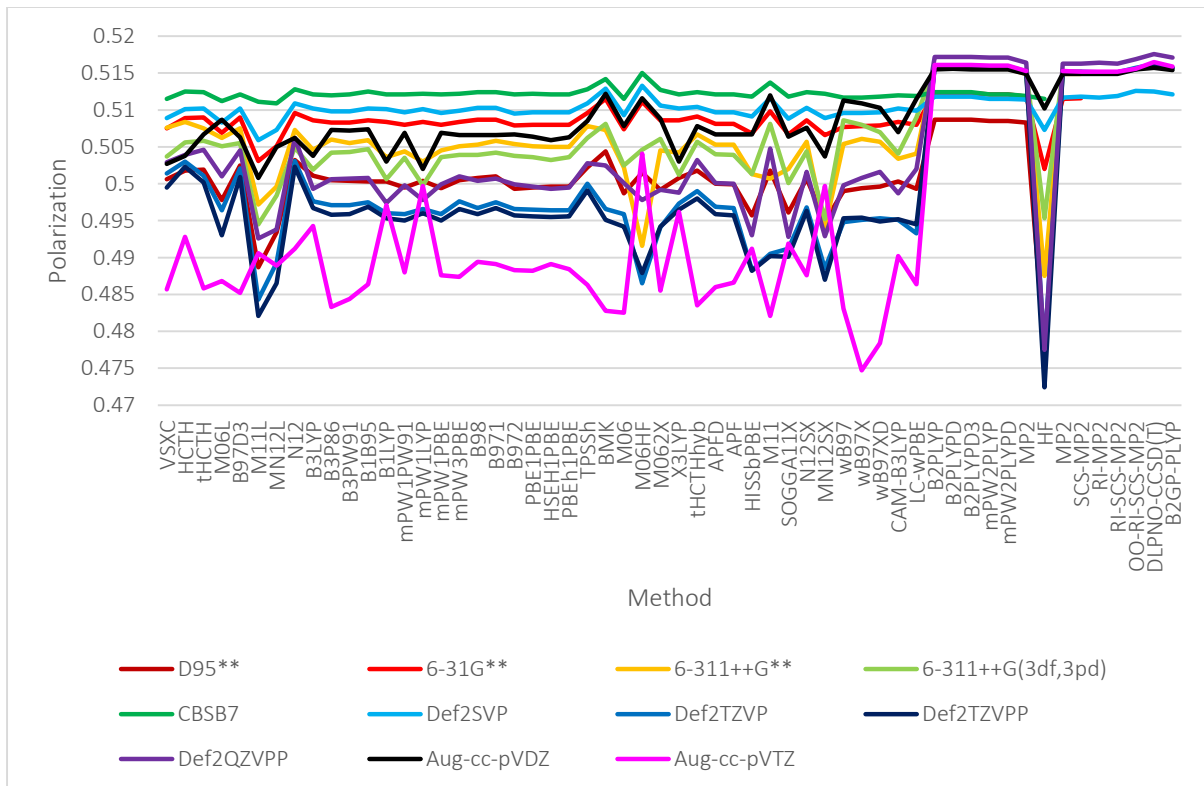


Figure 28. C-C(σ) Central Carbon NHO Polarization in Vinylamine at 10 Degree C-C-N-H Torsion with Varying Method and Basis Set

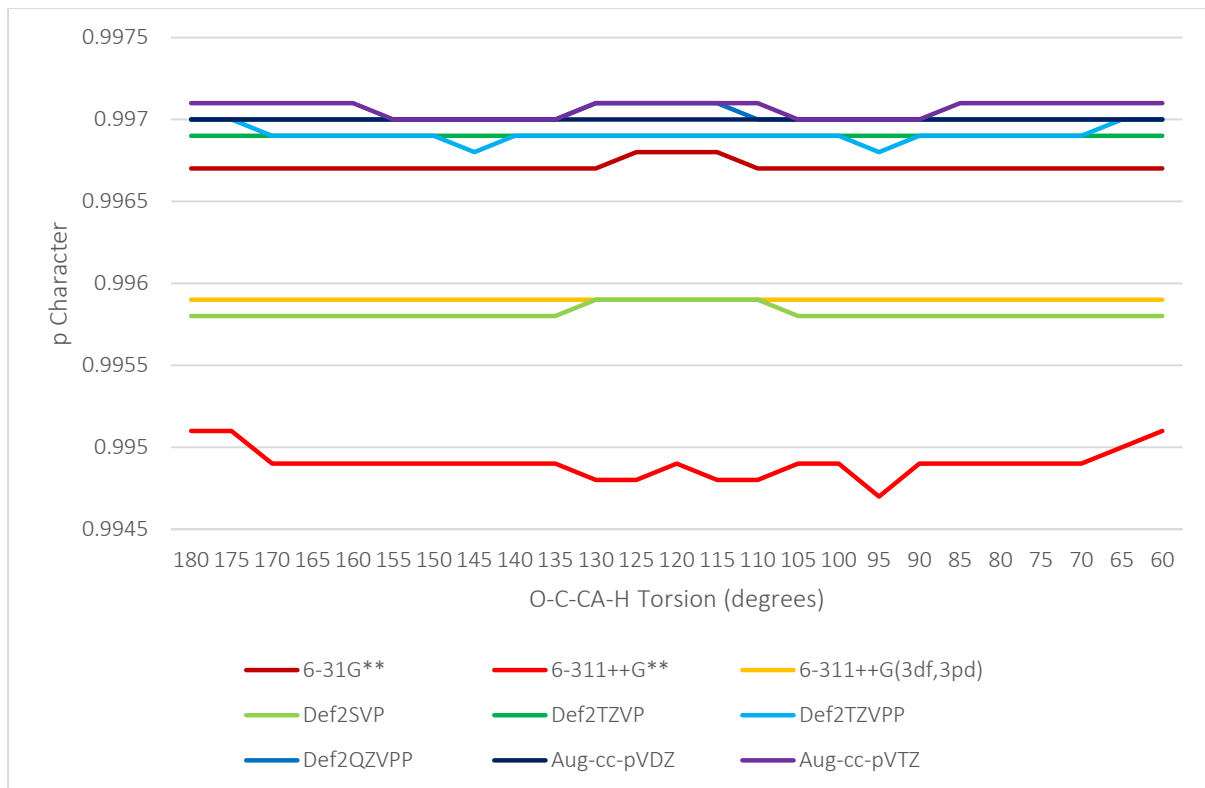


Figure 29. $C\text{-}O(\pi)$ Carbon NHO p Character in Ethanamide at Varying O-C-CA-H Torsion and Basis Set at MP2

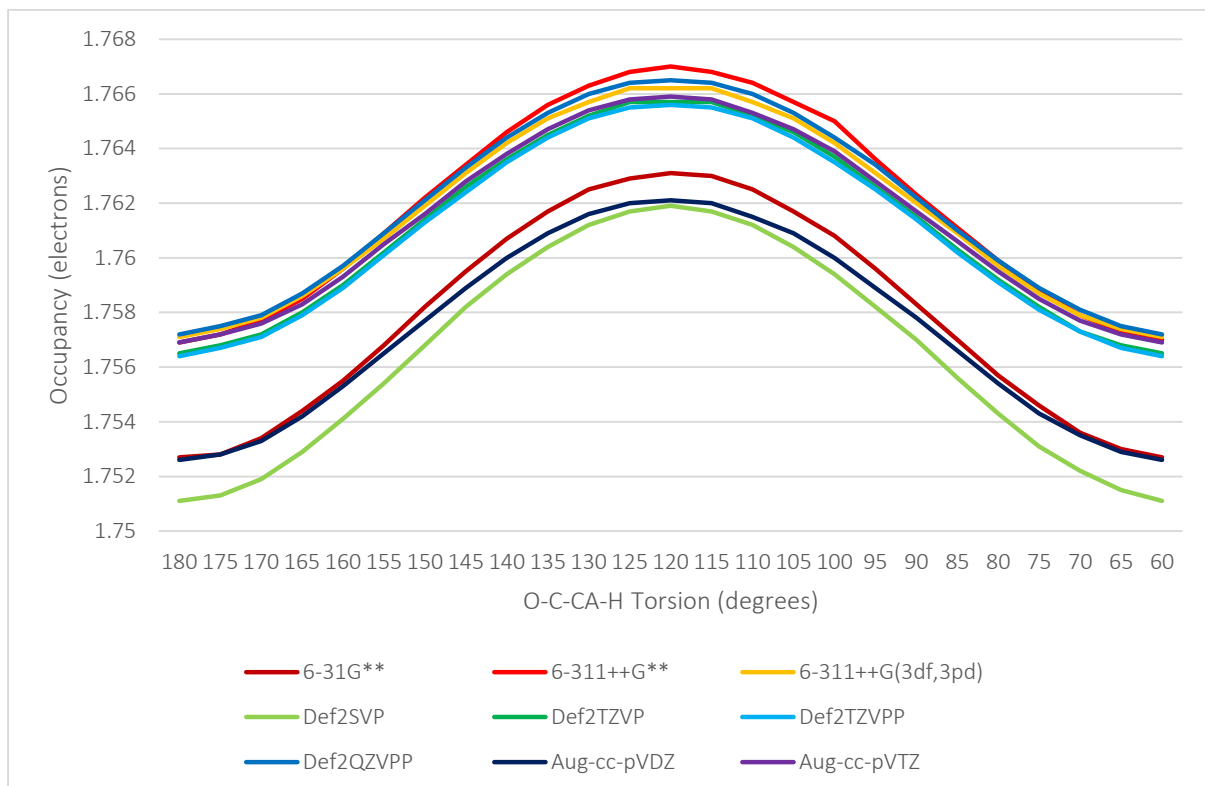


Figure 30. Nitrogen Lone Pair NBO Occupancy in Ethanamide at Varying O-C-CA-H Torsion and Basis Set at B3LYP

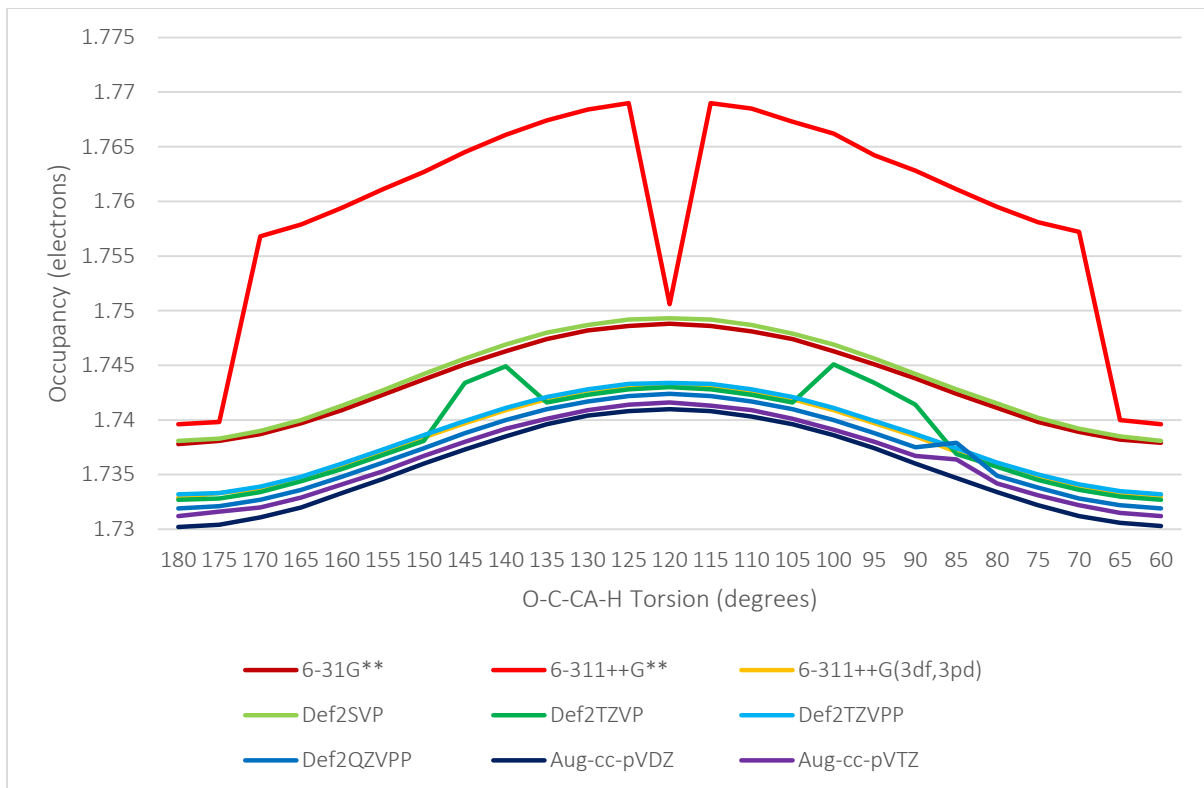


Figure 31. Nitrogen Lone Pair NBO Occupancy in Ethanamide at Varying O-C-CA-H Torsion and Basis Set at MP2

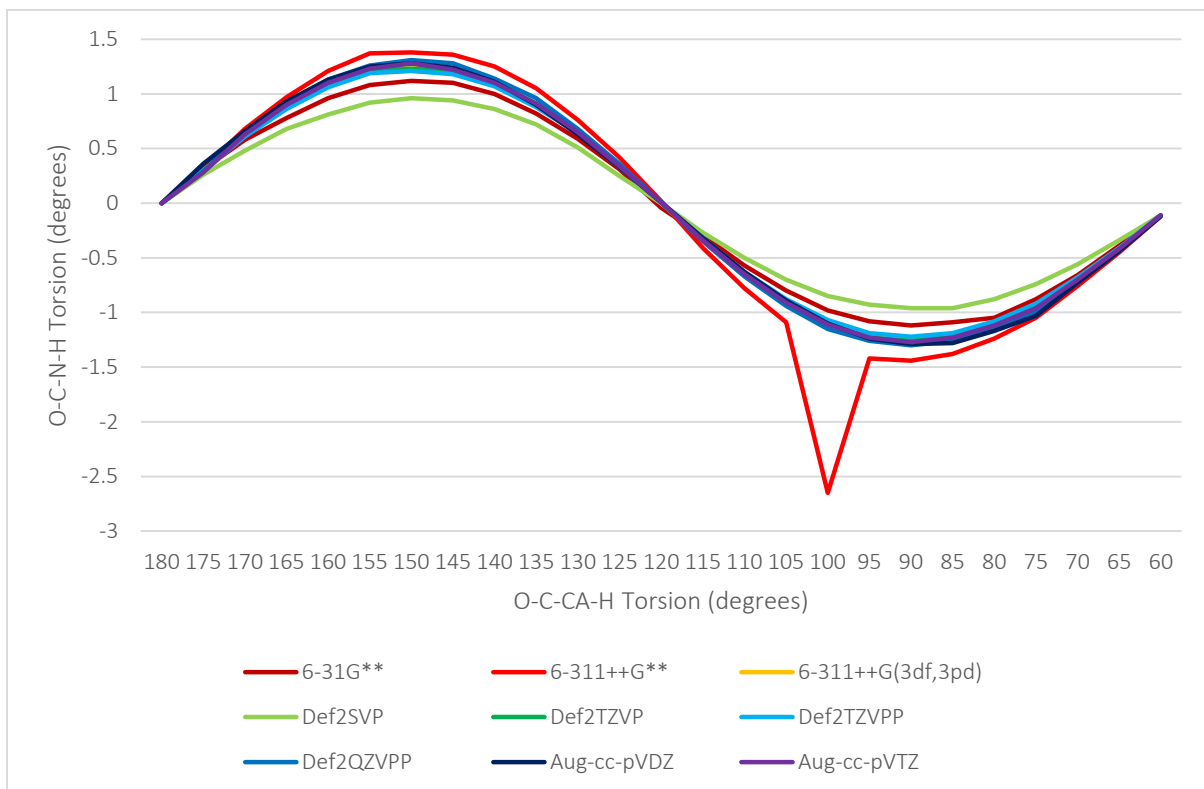


Figure 32. O-C-N-H Torsion in Ethanamide with Varying O-C-CA-H Torsion and Basis Set at B3LYP

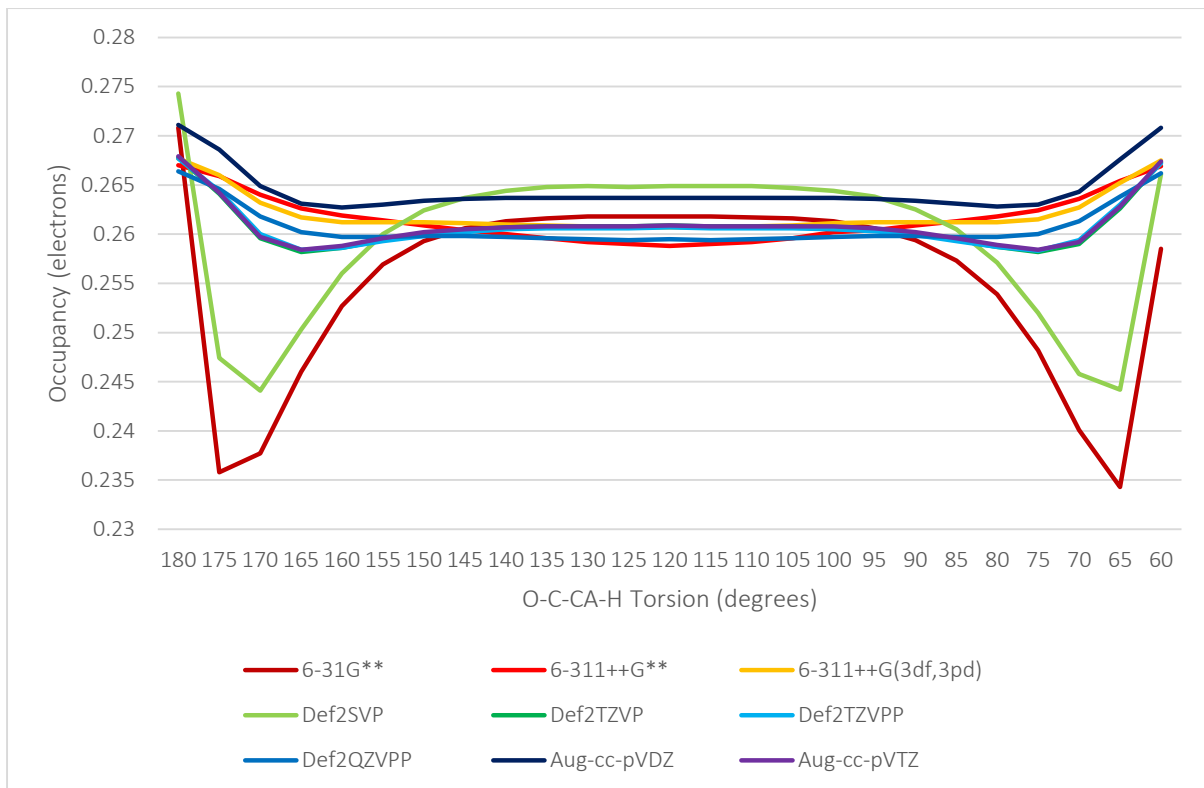


Figure 33. C-O(π)* NBO Occupancy at Varying O-C-CA-H Torsion and Basis Set at B3LYP

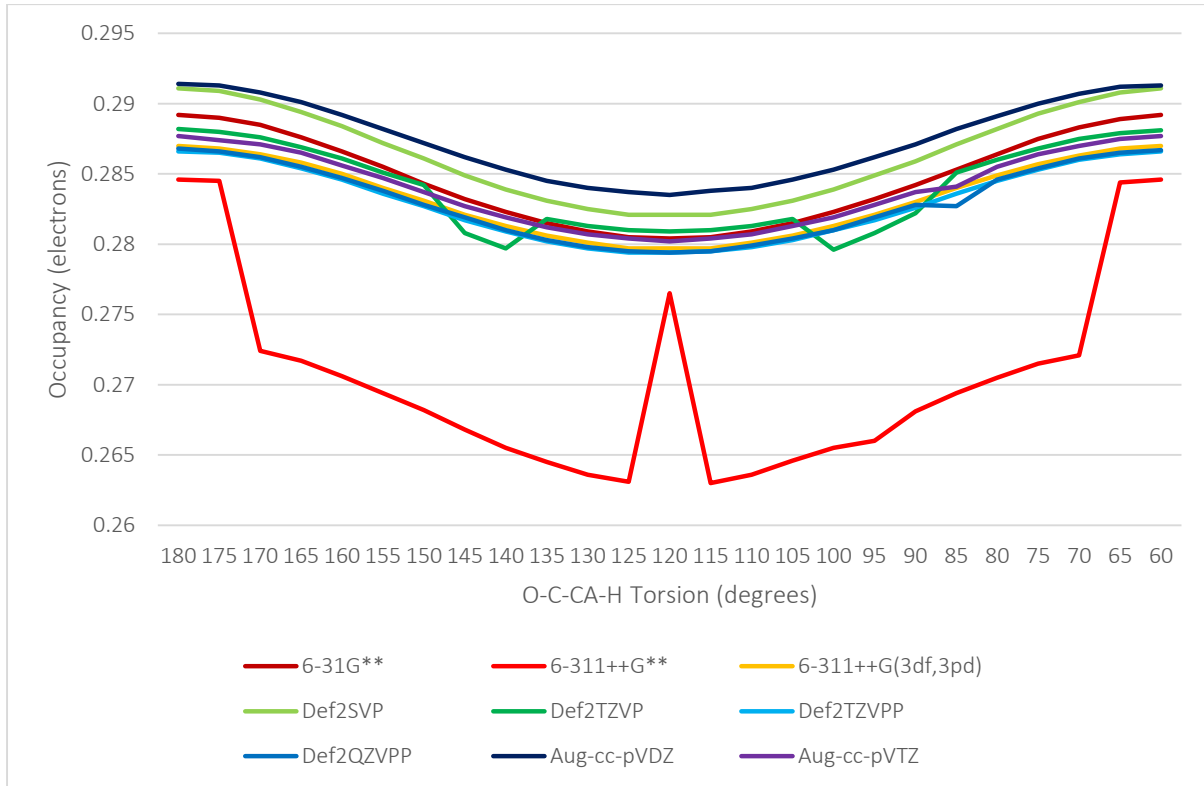


Figure 34. C-O(π)* NBO Occupancy at Varying O-C-CA-H Torsion and Basis Set at MP2

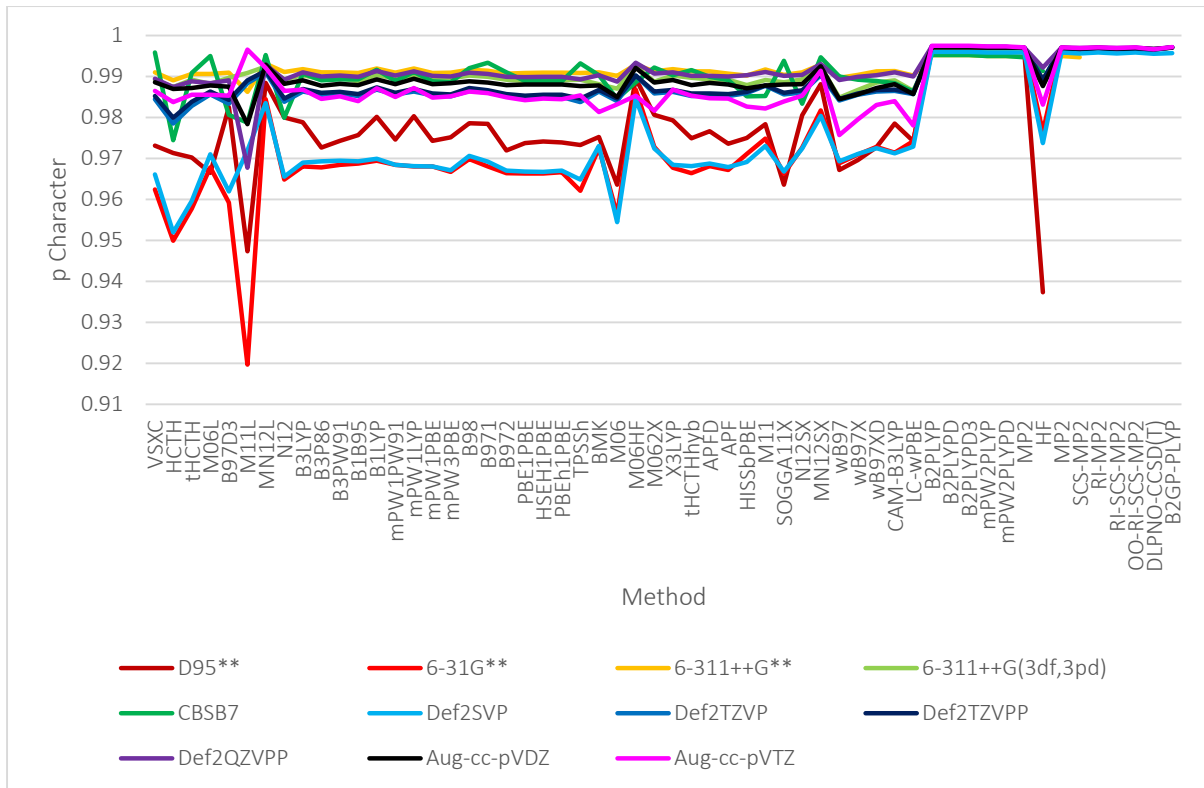


Figure 35. C-O(pi) Carbon NHO p Character in Ethanamide at Antiparallel Beta Strand Psi Torsion with Varying Method and Basis Set

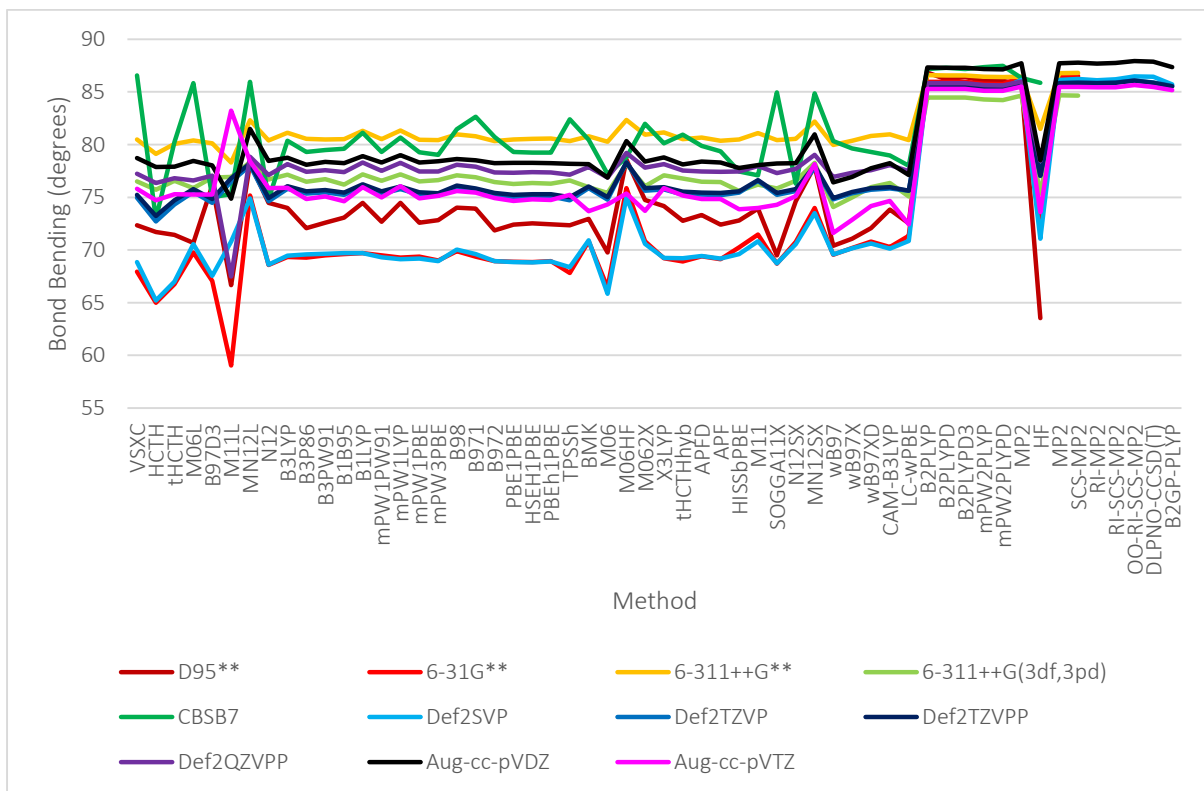


Figure 36. C-O(pi) Carbon NHO Bond Bending at Antiparallel Beta Strand Psi Torsion with Varying Method and Basis Set

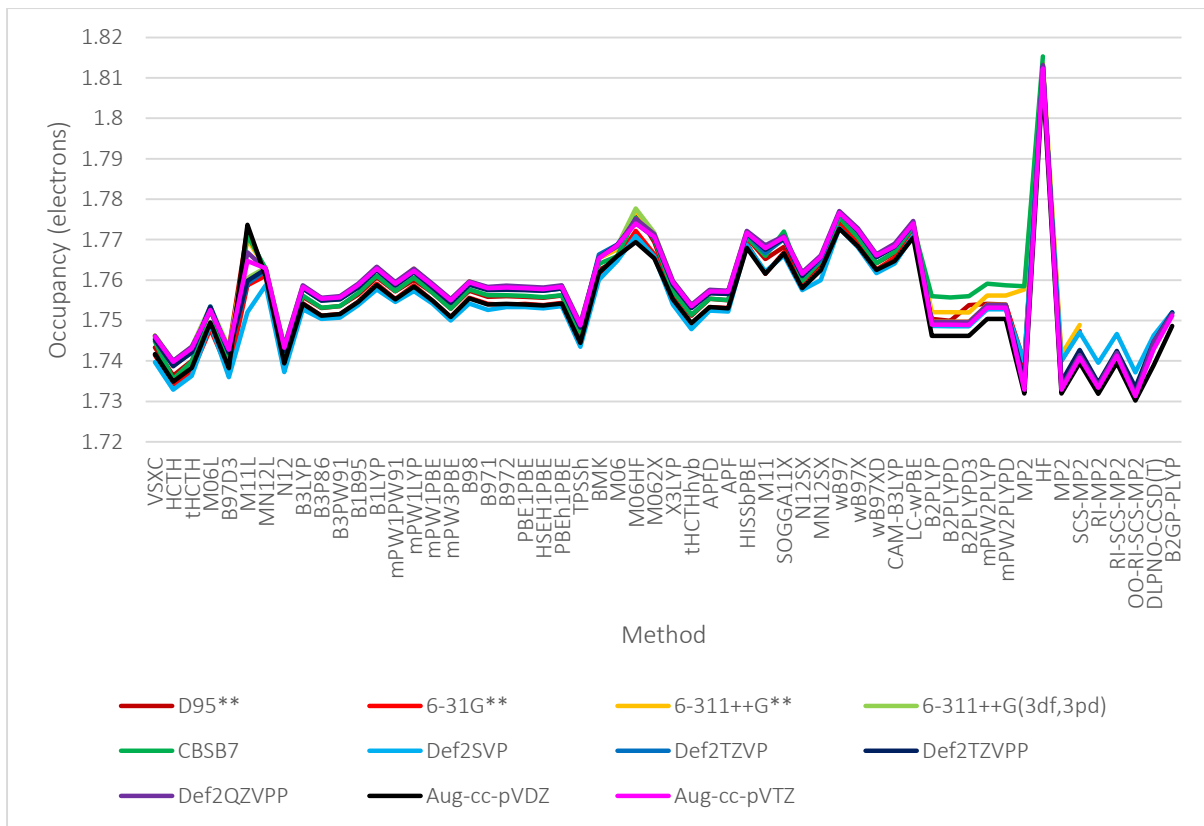


Figure 37. Nitrogen Lone Pair NBO Occupancy in Ethanamide at Antiparallel Beta Strand Psi Torsion with Varying Method and Basis Set

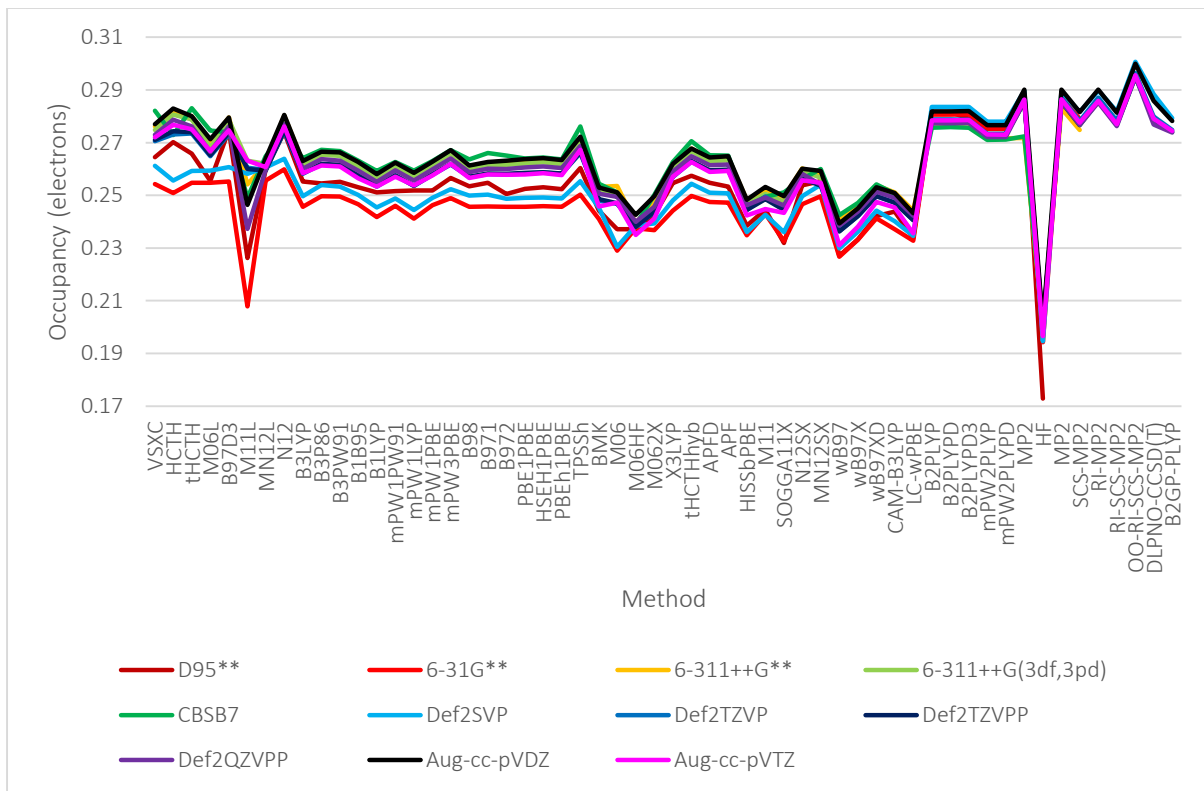


Figure 38. C-O(π)* NBO Occupancy in Ethanamide at Antiparallel Beta Strand Psi Torsion with Varying Method and Basis Set

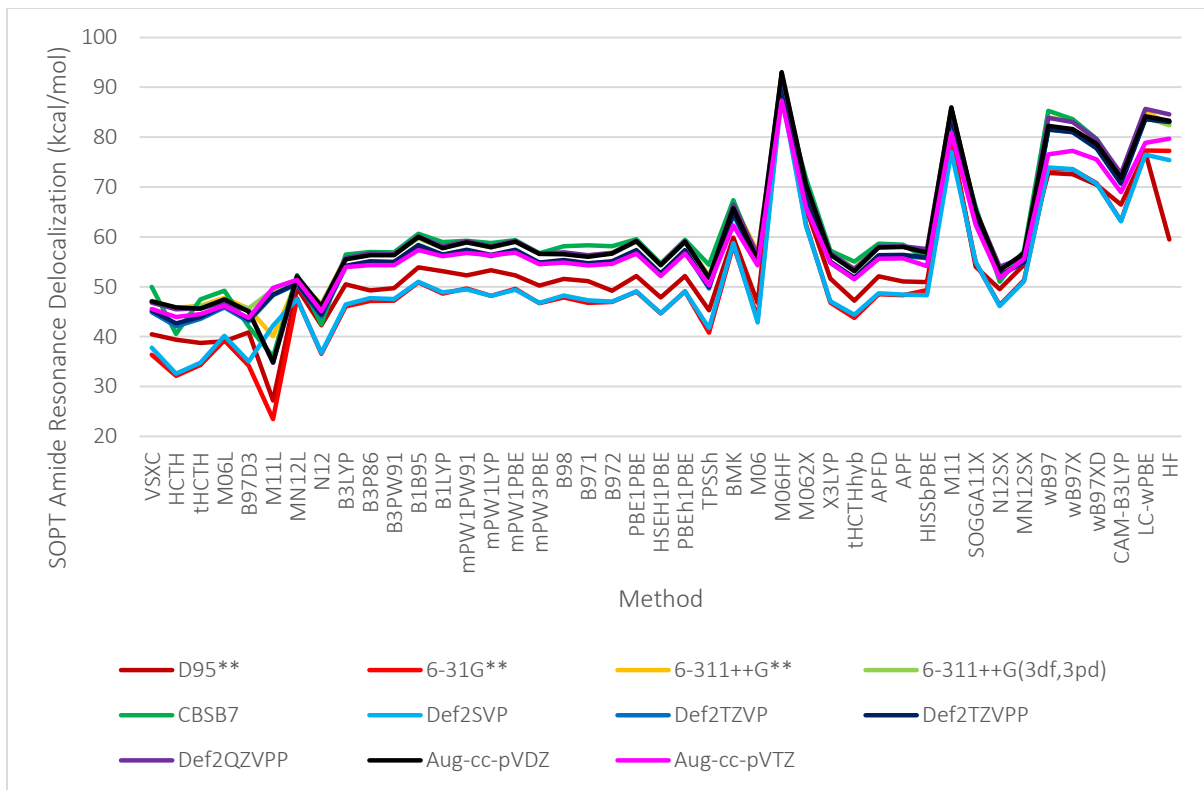


Figure 39. Second Order Perturbation Theory Amide Resonance Delocalization ($N(LP) \rightarrow C-O(\pi^*)$) in Ethanamide at Antiparallel Beta Strand Psi Torsion and Varying Method and Basis Set

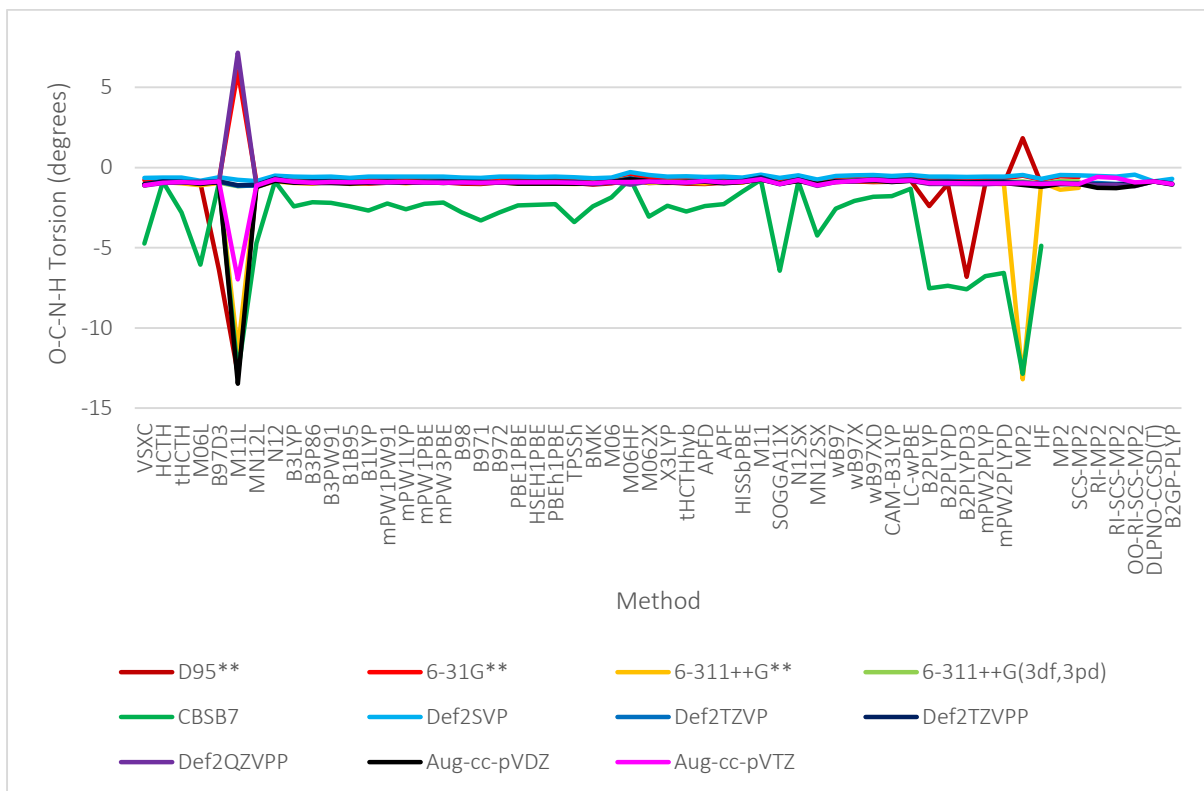


Figure 40. O-C-N-H Torsion in Ethanamide at Antiparallel Beta Strand Psi Torsion with Varying Method and Basis Set

Appendix 2

Table 1. CASSCF(8,7)/MRCI+Q TZVPP ethanamide symmetry and bond bending at beta sheet psi torsions

Beta Psi Torsion	Energy at Ground	Largest p Character Bond Bending		
		Config Weight	of C-O(p) C NHO	of C-O(p) C NHO
Parallel	-208.862366	0.8435	0.9968	86.2
Antiparallel	-208.871637	0.8387	0.9968	86.2

Table 2. Dihedral Angles (degrees) in Ethanamide with O-C-CA-H Constrained to -165 at MP2/6-311++G** with CP Fragment Boundaries at Bond Shown

Fragment	O-C-N-H1	O-C-N-H2
none	-163.359	-13.248
C-C	-165.651	-11.899
C-N	178.312	-0.373

- s: s character of C-O(pi)* Carbon NHO
- p: p character of C-O(pi)* Carbon NHO
- d: d character of C-O(pi)* Carbon NHO
- Dev: bond bending of C-O(pi)* Carbon NHO (degrees)
- Dih: O-C-CA-HA dihedral angle
- PolP: polarization of C-O(pi) NBO
- PolS: polarization of C-O(sigma) NBO
- CoapOcc: occupancy of C-O(pi)* NBO
- CoasOcc: occupancy of C-O(sigma)* NBO
- SoptP: N(LP)->C-O(pi)* SOPT (kcal/mol)
- SoptS: N(LP)->C-O(sigma)* SOPT (kcal/mol)
- CaHaCos: CA-HA->C-O(sigma)* SOPT (kcal/mol)
- CaCbCop: CA-CB->C-O(pi)* SOPT (kcal/mol)
- CaNCop: CA-N->C-O(pi)* SOPT (kcal/mol)
- CopCaN: C-O(pi)>Ca-N* SOPT (kcal/mol)
- Cid: identity of Carbon atom central to backbone amide group
- Strand: beta strand in sheet
- Chain: cross-strand hydrogen bonding chain

Figure 41. Column Names for Table 3 and Table 4

Table 3. Polyvaline Antiparallel Beta Sheet Backbone Amide Resonance Delocalization, Bond Bending and Loss of sigma/pi Symmetry at LC-wPBE/6-31G**

s	p	d	Dev	Dih	PolP	PolS	CoasOcc	CoapOcc	SoptP	SoptS	CaHaCos	CaCbCop	CaNCop	CopCaN	Cid	Strand	Chain
0.0452	0.9514	0.0034	65.33	179.3	0.2698	0.3348	0.058	0.2841	88.32	7.33	5.16	2.98			80	2	1
0.0436	0.953	0.0034	65.66	-180	0.2693	0.335	0.0566	0.2854	89.32	7.05	5.23	3.12			158	3	4
0.0226	0.9742	0.0032	70.86	158.1	0.2895	0.3465	0.0347	0.2583	85.52	4.28	3.71				2	1	4
0.0214	0.9754	0.0032	71.29	158.7	0.2891	0.3469	0.0333	0.2603	87.24	3.85	3.8	1.03			236	4	1
0.0105	0.9859	0.0036	76.24	-165.6	0.2651	0.3424	0.0241	0.3	110.91	1.36	5.38	4.42	2.01		252	4	1
0.0096	0.9869	0.0036	76.78	-166	0.2644	0.3427	0.0229	0.3013	111.94	1.18	5.38	4.42	2.01		18	1	3
0.0034	0.993	0.0036	82.1	-171.8	0.2699	0.3453	0.0177	0.2961	112.24		4.83	4.1	2.22	1.05	50	1	1
0.0023	0.9942	0.0036	83.4	-170.6	0.2695	0.3454	0.0166	0.2968	113.23		4.83	4.27	2.16	1.01	284	4	4
0.0009	0.9957	0.0034	83.84	-167.5	0.2821	0.3504	0.0149	0.2901	111.74		4.53	4.41	1.85		268	4	3
0.0006	0.996	0.0034	84.45	-168.4	0.2821	0.3505	0.0145	0.2907	112.24		4.57	4.34	1.96		34	1	2
0.0005	0.9958	0.0037	85.07	-164.9	0.2586	0.3443	0.0166	0.3258	128.3		4.76	5.03	1.62		96	2	2
0.0002	0.9961	0.0037	86.16	-164.1	0.2582	0.3445	0.016	0.3265	128.93		4.81	5.06	1.6		174	3	3
0.0002	0.9961	0.0037	86.35	-165.3	0.2608	0.3447	0.0159	0.3235	127.29		4.8	5.17	1.59		190	3	2
0.0001	0.9962	0.0037	86.93	-165.7	0.2607	0.3447	0.0156	0.3235	127.48		4.84	5.21	1.58		112	2	3
0.0003	0.9961	0.0036	87.46	-173	0.2639	0.3455	0.0154	0.3234	128.47		5.07	4.2	2.1	1.12	128	2	4
0.0002	0.9962	0.0036	87.84	-173.6	0.2639	0.3456	0.0153	0.3233	128.45		5.05	4.13	2.17	1.14	206	3	1

Table 4. Polyalanine Antiparallel Beta Sheet Backbone Amide Resonance Delocalization, Bond Bending and Loss of sigma/pi Symmetry at LC-wPBE/6-31G**

s	p	d	Dev	Dih	PolP	PolS	CoasOcc	CoapOcc	SoptP	SoptS	CaHaCos	CaCbCop	CopCaCb	Cid	Strand	Chain
0.0215	0.9753	0.0032	71.5	-169.16	0.2922	0.3476	0.0344	0.2602	86.01	4.07	4.71			64	1	6
0.0158	0.981	0.0032	73.75	-171.07	0.2905	0.3488	0.0288	0.2662	91.11	2.91	4.94			168	4	1
0.0139	0.9826	0.0035	73.78	-151.02	0.2784	0.3433	0.0292	0.2744	96.89	3.13	3.42	4.72	1.13	133	4	6
0.0124	0.9841	0.0035	74.47	-149.44	0.2785	0.3437	0.0275	0.2753	98.12	2.79	3.36	4.74	1.16	26	1	1
0.0131	0.9833	0.0036	74.73	-175.2	0.2615	0.3428	0.0275	0.3139	113.01	1.71	5.75			48	2	1
0.0099	0.9865	0.0036	76.42	-173.57	0.2607	0.3434	0.0242	0.3163	115.78	1.19	5.75			184	3	6
0.0076	0.9888	0.0036	78.23	-134.89	0.2674	0.3453	0.0204	0.302	112.74	1.36	4.24	6.38	1.66	123	4	4
0.0057	0.9906	0.0036	79.42	-134.25	0.2665	0.3458	0.0187	0.3047	115.6		4.08	6.2	1.64	32	1	3
0.0039	0.9926	0.0035	79.8	-135.81	0.2817	0.3503	0.018	0.2859	106.46	1.54	2.67	4.34	1.44	128	4	5
0.0032	0.9933	0.0035	80.37	-137.2	0.2813	0.3506	0.0172	0.2872	108.25	1.24	2.8	4.59	1.45	21	1	2
0.0025	0.994	0.0035	81.11	-138.34	0.2815	0.3511	0.0164	0.2887	110.49		2.98	4.71	1.49	55	1	4
0.0025	0.9941	0.0035	81.26	-137.36	0.2815	0.351	0.0162	0.2887	110.48		2.91	4.63	1.49	170	4	3
0.0035	0.9928	0.0037	81.37	-141.14	0.2623	0.3454	0.0169	0.308	118.71		4.55	6.59	1.57	163	4	2
0.0034	0.993	0.0037	81.59	-143.92	0.262	0.3453	0.0169	0.3083	119.06		4.68	6.63	1.54	59	1	5
0.0017	0.9946	0.0037	83.76	-145.73	0.261	0.3458	0.0153	0.3218	127.37		4.37	6.14	1.5	50	2	3
0.0013	0.995	0.0037	84.27	-144.83	0.2611	0.3459	0.015	0.3217	127.45		4.3	6.07	1.51	175	3	4
0.0012	0.9951	0.0037	84.47	-143.88	0.262	0.3466	0.0149	0.3209	126.95		4.25	6.21	1.53	152	3	3
0.0008	0.9955	0.0037	85.21	-144.36	0.262	0.3465	0.0147	0.3213	127.31		4.21	6.13	1.51	4	2	4
0.0007	0.9955	0.0037	85.4	-145.35	0.257	0.3453	0.0151	0.3258	129.51		4.37	6.17	1.46	179	3	5
0.0006	0.9956	0.0037	85.55	-143.09	0.2576	0.3456	0.015	0.3248	128.93		4.26	6.08	1.49	43	2	2
0.0004	0.9958	0.0038	86.19	-147.33	0.2578	0.3455	0.0147	0.3286	130.93		4.27	6.05	1.42	141	3	2
0	0.9964	0.0036	86.58	-150.1	0.2696	0.347	0.0145	0.3103	122.22		4.34	5.89	1.43	14	2	6
0.0003	0.9961	0.0036	86.67	-150.96	0.2696	0.3472	0.0143	0.3108	122.79		4.47	5.98	1.44	146	3	1
0.0001	0.9974	0.0025	88.02	-146.83	0.7422	0.6546	0.0147	0.3285	130.83		4.26	6.05	1.43	9	2	5